Contents lists available at ScienceDirect

Atmospheric Research

journal homepage: http://ees.elsevier.com

# Sensitivity analysis of the WRF model: Assessment of performance in high resolution simulations in complex terrain in the Canary Islands

David Suárez-Molina [a], Sergio Fernández-González [a,*], Gustavo Montero [b], Albert Oliver [b], Juan Carlos Suárez González [a]

[a] State Meteorological Agency (AEMET), Spain
[b] University Institute for Intelligent Systems and Numerical Applications in Engineering (SIANI), University of Las Palmas de Gran Canaria, Spain

ARTICLE INFO

*Keywords*
WRF
Sensitivity analysis
Complex terrain
PBL
Microphysics
Canary Islands

ABSTRACT

Canary Islands and other regions have been greatly damaged by weather events during the last decades. For this reason, the main duty of National Meteorological Services is to minimize socio-economic losses by forecasting adverse weather episodes with enough time in advance. To achieve this goal, the use of numerical weather prediction models is highly relevant. And, even more crucial, is to comprehend the model accuracy.In this paper, an exhaustive sensitivity analysis of the Weather Research and Forecasting (WRF) model over the Canary Islands has been carried out. The complex terrain of the archipelago makes the islands a test bench of high interest. Four scores were used to assess the accuracy of the model configurations: Bias, mean absolute error (MAE), root of the Mean Squared Error (RMSE), and the correlation coefficient (r). Initially, twenty-five WRF model configurations were considered. However, a preliminary test discarded inadequate configurations, and reduced the number to six. The variables of interest were air temperature at 2 m (T2m), maximum 1-h wind gust at 10 m and 3-h rainfall accumulation. The results indicated a systematic wind speed underestimation. This underestimation is related to the influence of the location and the complex orography. The most accurate wind forecasts were obtained using the Mellor-Yamada-Janjic Planetary Boudary Layer (PBL) scheme with the WSM6 microphysics (MP) scheme. Another major conclusion is that, for precipitation, the PBL scheme has a greater impact than the MP scheme. Finally, the results show that the Boulac – Thompson combination is the most accurate regarding T2m forecast.

## 1. Introduction

Extreme weather events have negative impacts on transportations and communications, consequently resulting in catastrophic effects on distinct aspects of people's lives and economy. Despite the apparent climatic mildness, the frequency and intensity of the severe weather events have serious consequences on the Canary Islands (Dorta, 2007). To understand this impact, statistics show that severe weather events caused 74 fatalities between 1995 and Eiserloh, 2014 (Suárez-Molina et al., 2018). According to the CCS ("Consorcio de Compensación de Seguros", a public organization funded by the Ministry of Economy, Industry and Competitiveness of the Spanish Government), between 1996 and 2018, floods and windstorms in the Canary Islands produced more than 211 million Euros in losses (Suárez-Molina et al., 2020).

The accuracy of Numerical Weather Prediction (NWP) models in complex terrain is lower than over flat and homogeneous terrain. This discrepancy is attributed to the fact that boundary-layer processes in complex terrain are not well represented by NWP models. Previous studies have evaluated the performance of different planetary boundary layer (PBL) parameterization schemes in locations known for complex atmospheric situations (Pérez et al., 2006; Bossioli et al., 2009). Microphysics schemes in numerical models play a key role in simulating the formation of cloud droplets, precipitation, and land surface temperature. It also takes into account the interactions and energy fluxes between the atmosphere and the surface, which is considered a key parameter in many hydrological, meteorological and environmental studies (Anderson et al., 2011).

In recent years, the use of the Weather Research and Forecasting (WRF) model in operational mode has increased. For instance, since 2017, the National Centers for Environmental Prediction (NCEP) use in operational mode the Hurricane Weather Research and Forecast (HWRF) system (Biswas et al., 2018). In addition, the WRF model has been used by other authors in operational mode with different purposes (Hsiao et al., 2012; Hamill, 2014; Sahoo et al., 2019). The WRF model is also being used in γSREPS, an Ensemble Prediction Sys-

* Corresponding author.
*E-mail address:* sfernandezg@aemet.es (S. Fernández-González)

https://doi.org/10.1016/j.atmosres.2020.105157
Received 19 June 2020; Received in revised form 13 July 2020; Accepted 22 July 2020
Available online xxx
0169-8095/

tem developed by AEMET, the Spanish Meteorological Agency (Callado et al., 2019).

Although other studies have used WRF in the Canary Islands for particular phenomena (Marrero et al., 2008; Jorba et al., 2015; Quitián-Hernández et al., 2018), a comprehensive sensitivity analysis has not been carried out before. Such study is essential to determine the most convenient model setup for this geographical domain (Borge et al., 2008). In addition, it should be taken into consideration that the operational forecast of convective episodes is more problematic in subtropical regions such as the Canary Islands (Žagar et al., 2005).

The purpose of this work is to evaluate the quality of WRF forecasts in the Canary Islands. The fields analyzed–air temperature at 2 m (T2m), maximum 1-h wind gust at 10 m and 3-h rainfall accumulation–are of vital importance for issuing meteorological warnings (METEOALERTA, 2018). The period analyzed (15 days in February 2018) includes various weather patterns; therefore, the sensitivity analysis will evaluate the model performance under different atmospheric conditions.

This paper is structured as follows: Section 2 describes the study area, the configuration of the WRF experiments and the observational dataset used to evaluate the model performance. Section 3 presents the results of the performance evaluation. Finally, Section 4 summarizes the paper conclusions.

## 2. Methodology

### 2.1. Study area and dataset

This research is focused on the Canary Islands (Fig. 1). This archipelago is in front of the west coast of North Africa in the subtropical zone (27°37′–29°25′N and 18°10′–13°20′W). The archipelago is formed by seven islands of volcanic origin that present a complex orography. The highest point is Mount Teide (3718 m) on Tenerife (TF). With Tenerife being by far the highest island, La Palma (LA), Gran Canaria (GC), La Gomera (GO) and El Hierro (HI) constitute a medium cluster with highest heights of: 2423 m (Roque de los Muchachos, LA), 1948 m (Pico de Las Nieves, GC), 1501 m (Pico de Malpaso, HI) and 1487 m (Garajonay, GO). Lanzarote (LZ) and Fuerteventura (FV) are much flatter with maximum heights of 671 m and 807 m, respectively.

#### 2.1.1. Episode selection

Analysis is conducted for two periods of February 2018: from February 1st at 00 h UTC to February 11th at 12 h UTC, and from February 23rd at 00 h UTC to February 28th at 12 h UTC. This approach allows the evaluation of the meteorological model under different atmospheric conditions. The synoptic situation during the different episodes of the study period will be described below:

**1–4 February 2018:** High pressure system centered north of the Azores Islands with central pressures exceeding 1038 hPa. Northeasterly winds were predominant. During February 1st and 2nd, a cut-off low system affected the Canary Islands.
**5** February **2018:** Low pressure system of 1008 hPa over Algeria generated weak pressure gradient across Canary archipelago
**6–11 February 2018:** Strong high pressure system centered near to Azores Islands with central pressures about 1040 hPa. The Canary Islands were located eastwards of the ridge.
**23–28 February 2018:** Different low pressure systems moving from Azores to the Canary Islands with central pressures about 966–1000 hPa. A cold front affected the islands on February 24 and 25. The prevailing winds were from the west.

### 2.2. WRF model configurations

The model used is the version 3.9.1 of the Advanced Research version of WRF (ARW), a fully compressible and nonhydrostatic model. Two different vertical coordinate systems are available: terrain-following coordinate (TFC) and hybrid vertical coordinate (HVC) hydrostatic pressure coordinate. The Arakawa C-grid staggering is used. The model includes the Runge-Kutta 2nd and 3rd order time integration schemes, and 2nd to 6th order advection schemes in both horizontal and vertical directions. It also applies a time-split small step for acoustic and gravity-wave modes. Dynamics conserves scalar variables. This model is described in more detail in Skamarock et al. (2008).

Boundary conditions and initial starting conditions were derived from the Operational Dataset HRES-IFS (High Resolution-Integrated Forecasting System, from ECMWF) with 0.09° x 0.09° spatial resolution and temporal resolution of 3 h. Each of the 15 days analyzed were run individually, following recommendations of similar sensitivity analysis (Evans et al., 2012; Johnson and Wang, 2012; Fernández-González et al., 2015, 2017; García-Ortega et al., 2017). The lead time of the simulations is 36 h, considering the first 12 h as spin-up time; hourly outputs were generated.

The simulations consist of three nested domains (Fig. 2) following a two-way nesting strategy, with spatial resolutions of 9 (d01), 3

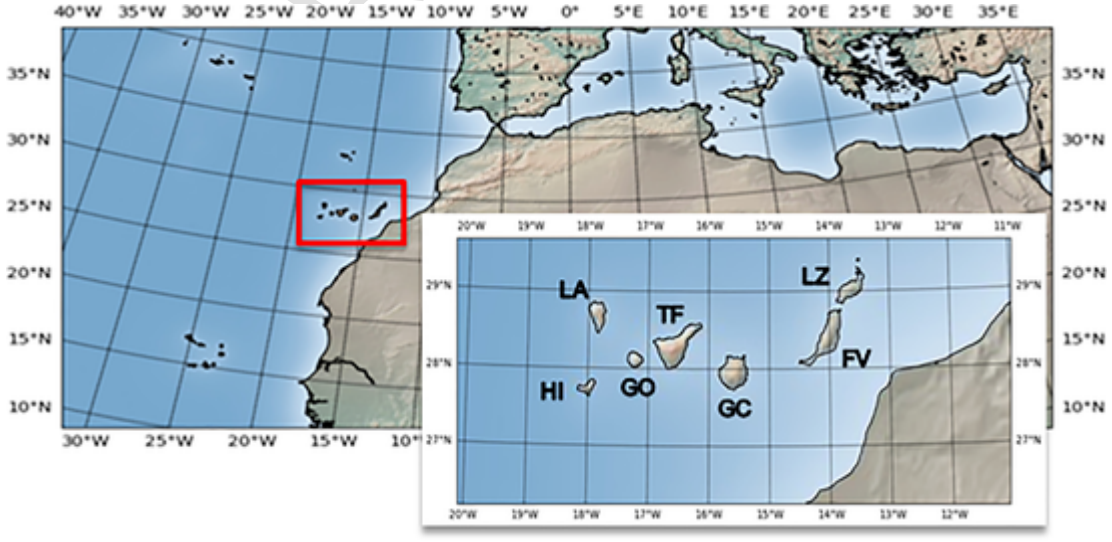


**Fig. 1.** Location of Canary Islands in the Subtropical Eastern Atlantic. The zoom shows the study area in more detail.

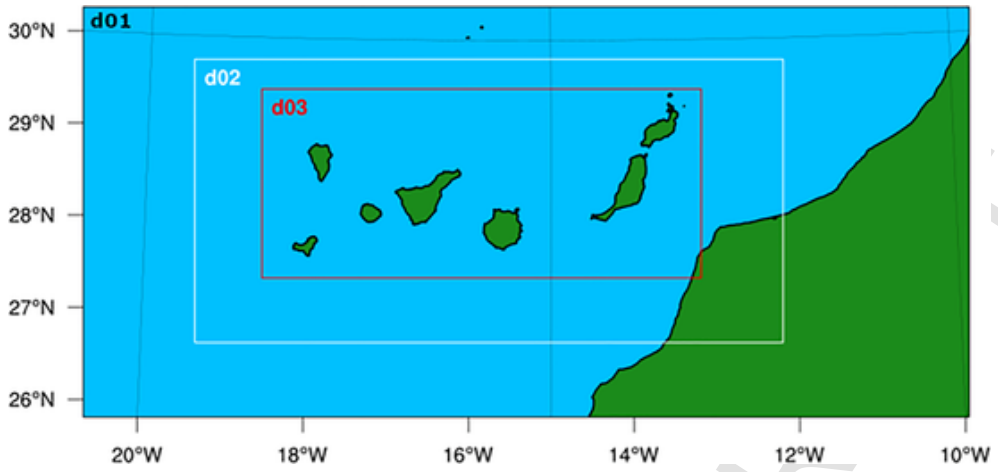


**Fig. 2.** Domains with spatial resolutions of 9 (d01), 3 (d02) and 1 km (d03).

(d02) and 1 km (d03), respectively. Forty sigma levels in the vertical axis were selected.

The WRF model offers several options to configure physics schemes, enabling optimization of the model for specific weather phenomenon and study area. The parameterization schemes were selected based upon previous works with similar conditions of complex terrains (Moya-Alvarez et al., 2018; González Rocha et al., 2017; Evans et al., 2012).

For radiation, the RRTMG (Iacono et al., 2008) longwave and shortwave schemes were used. It is a new version of RRTM (added in WRF Version 3.1) and includes the MCICA method of random cloud overlap. Radiation was called every 10 min. The surface processes were parameterized by the Noah Land Surface Model (NLSM), a four-layer soil temperature and moisture scheme that provides data of sensible and latent heat fluxes in the PBL (Chen and Dudhia, 2001).

The WRF Model determines surface heat, momentum, and moisture fluxes mainly via the PBL scheme, which estimates wind shear and friction at the subgrid-scale (Fernández-González et al., 2018). For this reason, five PBL scheme are evaluated to determine which one achieves the most realistic simulation for the variables of interest: the Yonsei University (YSU) (Hong et al., 2006), the Mellor-Yamada-Janjic (MYJ) (Janjic, 1994), the Mellor-Yamada-Nakanishi-Niino (MYNN2) (Nakanishi and Niino, 2006), The Asymmetric Convective Models (ACM2) (Pleim, 2007), and the BouLac (Bougeault and Lacarrere, 1989).

The YSU scheme is a first-order scheme that calculates turbulent fluxes using non-local eddy diffusivity coefficients. MYJ is an eta operational scheme with a one-dimensional prognostic turbulent kinetic energy scheme with local vertical mixing. MYNN2 predicts sub-grid TKE terms (new in Version 3.1 with a significant update in V3.8). ACM2 is the Asymmetric Convective Model with non-local upward mixing and local downward mixing. The BouLac PBL scheme is a one-and-a-half order, local closure scheme with a TKE prediction option designed for use with the BEP (Building Environment Parameterization) multi-layer, urban canopy model (Martilli et al., 2002). BouLac diagnoses PBL height as the height where the prognostic TKE reaches a sufficiently small value (in the current version of WRF is 0.005 $m^2s^{-2}$).

All these PBL schemes require the Monin-Obukhov (MO) surface-layer scheme, except MYJ that requires Eta similarity (MOJ). MO (MM5 similarity) is based on Monin-Obukhov with Carlson-Boland viscous sub-layer and standard similarity functions from look-up tables. In contrast, MOJ is based on Monin-Obukhov with Zilitinkevich thermal roughness length and standard similarity functions from look-up tables.

In addition, five different microphysics (MP) schemes are evaluated: Kessler (Kessler, 1969), WSM6 (Hong and Lim, 2006), Goddard (Tao et al., 1989), Thompson (Thompson et al., 2008) and Morrison (Morrison et al., 2009). Kessler is a warm-rain (i.e., no ice) scheme. WSM6, Goddar and Thompson are schemes with ice, snow and graupel processes suitable for high-resolution simulations. Morrison is a double-moment ice, snow, rain and graupel scheme for cloud-resolving simulations.

Cumulus parameterizations are not recommended for high horizontal resolutions. Therefore, in domains d02 and d03, the convective processes were resolved explicitly. On the other hand, the new Kain-Fritsch cumulus scheme (Kain, 2004) was applied to domain d01.

### 2.2.1. Initial test

Five different PBL and five different microphysics schemes were evaluated (Table 1) in order to know its impact in the T2m, precipitation and wind gust forecast. Twenty-five simulations (5 PBL × 5 MP_PHYSICS) were run for one day (these 25 experiments were called initial test). Initial test was chosen randomly. Then, according to bias and root squared mean error (RMSE), the best configurations were selected to run the remaining 14 days, avoiding increased computational cost. The selected configurations showed in average better results for all variables in initial test. The largest differences were obtained for wind gust. Bias for the selected configurations were about −3 km/h, while for the discarded configurations, the wind gust bias reached −7.50 km/h (for the combination MYNN2-Thompson). The combinations YSU-WSM6 and MYNN2-Kessler presented the largest bias for temperature (1 °C), whereas the selected configurations exhibited temperature bias closed to −0.6 °C). The selected configurations presented precipitation bias closed to 0 mm/h in initial test, while the largest bias was found for ACM2-Goddard (−0.25 mm/h).

**Table 1**
Summary of schemes used in initial test simulations.

| Radiation (shortwave/longwave) | Land surface model | PBL scheme - Surface layer | Microphysics scheme |
|---|---|---|---|
| RRTMG/RRTMG | NLSM | YSU-MO<br>MYJ-MOJ<br>MYNN2-MO<br>ACM2-MO<br>BouLac-MO | Kessler<br>WSM6<br>Goddard<br>Thompson<br>Morrison<br>2-Moment |

*2.2.2. Better performing configurations*

The initial test discarded inadequate combinations of parameterizations, keeping only six valid configurations for the sensitivity analysis. These valid configurations are the combination of three PBL schemes (MYJ, ACM2 and BouLac) with two microphysics schemes (WSM6 and Thompson); see Table 2.

*2.3. Sensitivity analysis methodology*

In order to verify the model results, observational data have been used. The observation data come from the AEMET observational network. This network is composed of 68 automatic meteorological stations (Fig. 3) across the Canary Islands. The data used in this paper are T2m, maximum 1-h wind gust at 10 m and 3-h rainfall accumulation. To evaluate the accuracy of the six model configurations, forecast verification of continuous predictands was carried out.

An hourly comparison between simulation results and observations (at the 68 automatic meteorological stations) was performed, except for precipitation where the 3-h rainfall accumulation was compared. For a given observational site, the simulation result is the closest grid point to the observational location. The validation was performed on D03, ensuring that the distance between the observation site and the closest grid point will always be less than 500 m. Although this can lead to representativeness errors, such errors are systematic in all simulations and do not play a significant role in the assessment of the relative model performance across model configurations (Jiménez et al., 2010).

According to other researchers (Pereira et al., 2013; Zhao and Zhang, 2018), a threshold for the 3-h rainfall accumulation validation should be established because there is a minimum measurable precipitation amount for the operational tipping bucket rain gauges. In this paper, it has been set to 0.2 mm in 3 h.

**Table 2**
Summary of combination of PBL and microphysics schemes selected.

| Setting code | PBL scheme - Surface layer | Microphysics (MP) scheme |
|---|---|---|
| Configuration 1 | MYJ-MOJ | WSM6 |
| Configuration 2 | ACM2-MO | WSM6 |
| Configuration 3 | BouLac-MO | WSM6 |
| Configuration 4 | MYJ-MOJ | Thompson |
| Configuration 5 | ACM2-MO | Thompson |
| Configuration 6 | BouLac-MO | Thompson |

In this research, the AFWA (the Air Force Weather Agency) diagnostic variable has been used for the maximum 10-m wind speed (afwa_diag_opt = 1). AFWA has made available to the WRF model a suite of diagnostics used in its operational Mesoscale Ensemble Prediction Suite (MEPS). The WSPD10MAX variable is used to parameterize surface wind gust (https://www2.mmm.ucar.edu/wrf/users/docs/AFWA_Diagnostics_in_WRF.pdf) applying the Weibull distribution .

Four scores were used to assess the accuracy of the model configurations: Bias, mean absolute error (MAE), root of the Mean Squared Error (RMSE), and the correlation coefficient ($r$). The model evaluation in the complex terrain will be presented by means of summary tables with overall results, scatter plots and through subsections lead time, geographical and vertical influence.

Bias represents the mean error and is the average of the difference between the forecast and the observation in each station and instant of time. The bias shows if the model overestimates the prediction (Bias $>0$) or underestimates it (Bias $<0$). It is important to note that it is not an accuracy measure, since it does not calculate the magnitude of individual forecast errors. It is computed as,

$$bias = \frac{1}{TN}\sum_{t=1}^{T}\sum_{i=1}^{N}\left(F_{i,t} - O_{i,t}\right)$$

where $F_{i,t}$ corresponds to the forecast value and $O_{i,t}$ to the observed value, both at the $i^{th}$ station in time $t$. The term T is the total number of hours and N the total number of stations.

Similarly, MAE is the arithmetic average of the absolute values of the differences between the members of each pair. MAE is zero for a perfect forecast and increases as discrepancies between the forecast and observations become larger. MAE can be interpreted as a typical magnitude for the forecast error in a given verification data set. The MAE formula is,

$$MAE = \frac{1}{TN}\sum_{t=1}^{T}\sum_{i=1}^{N}\left|F_{i,t} - O_{i,t}\right|$$

RMSE is the square root of the Mean Squared Error (MSE). MSE is the average squared difference between the forecast and observation pairs. Since the MSE is computed by squaring forecast errors, it will be more sensitive to larger errors than the MAE, and, thus, to outliers. RMSE has the same physical dimensions as forecasts and observa-

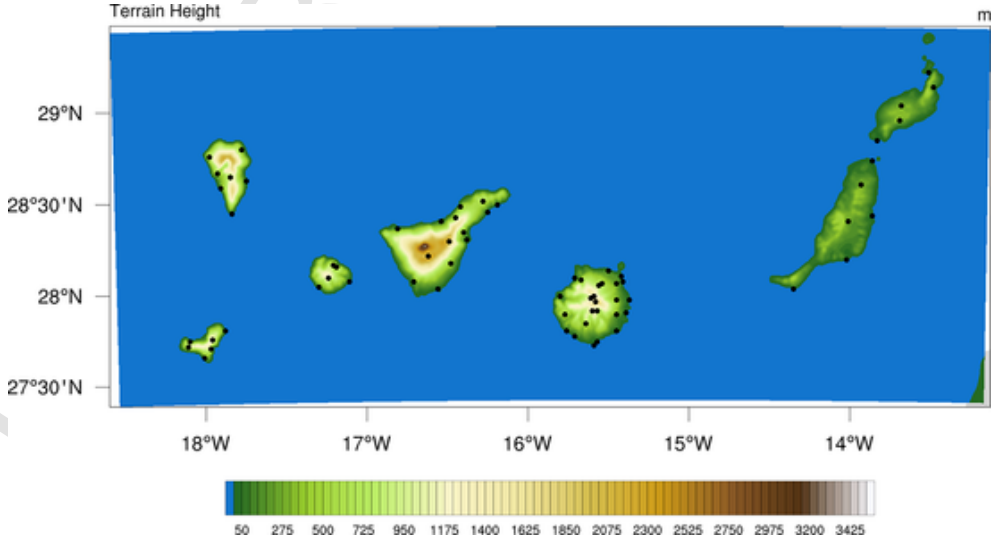


**Fig. 3.** Altitude within the domain 3 of the WRF model simulation. Automatic meteorological stations across the Canary Islands are marked by black dots.

tions and can be considered a magnitude for forecast errors. The formula for RMSE is,

$$RMSE = \sqrt{\frac{1}{TN}\sum_{t=1}^{T}\sum_{i=1}^{N}\left(F_{i,t} - O_{i,t}\right)^2}$$

Finally, $r$ is a good measure of linear association or phase error. The correlation measures the distance between the points of a scatter plot and the diagonal. It does not take into account forecast bias; therefore, a forecast with large errors may have a good correlation coefficient; however, the correlation coefficient is sensitive to outliers. It is computed as:

$$r = \frac{\sum_{t=1}^{T}\sum_{i=1}^{N}\left(F_{i,t} - \overline{F}\right)\left(O_{i,t} - \overline{O}\right)}{\sqrt{\sum_{t=1}^{T}\sum_{i=1}^{N}\left(F_{i,t} - \overline{F}\right)^2}\sqrt{\sum_{t=1}^{T}\sum_{i=1}^{N}\left(O_{i,t} - \overline{O}\right)^2}}$$

where $\overline{F}$ corresponds to the mean of forecasted values and $\overline{O}$ the mean of observed values.

## 3. Results and discussion

The results section is structured as follows; in Section 3.1 we will present the results of the sensitivity analysis where we discuss the different scores for the six configurations; then, we will study the dependency to the lead time (Section 3.2), to the location (Section 3.3), and altitude (Section 3.4).

### 3.1. Sensitivity analysis

The main objective of this study is to characterize model errors and to know the forecast accuracy in complex terrain. For these reasons, an overall evaluation has been carried out. Tables 3, 4 and 5 summarize estimated average values of the sensitivity analysis for all model configurations. The best values by score are highlighted in gray.

#### 3.1.1. Precipitation

The recorded mean (maximum) precipitation during the period studied oscillated from 1 to 10 (110) mm/day across the archipelago.

The different scores show some differences (Table 3). Configuration 1 was practically unbiased, while configuration 3 overestimated (bias $>0$), and the rest underestimated (bias $<0$). The best correlation between forecast and observation was also found in configuration 1. The lowest MAE and RMSE values were obtained in configuration 4. However, there are no large differences between all configurations (the differences are less than 1 mm in 3 h). Configurations 1 and 4 showed the best scores overall. Both have in common the PBL scheme (MYJ-MOJ) but differ in the MP scheme: WSM6 (configuration 1) and Thompson (configuration 4). All model configurations presented flow dependence and therefore the model skill depends on synoptic forcing. In general, the different model configurations overestimated the precipitation during weak synoptic forcing or under trade winds influence while underestimation occurred under strong synoptic forcing. In fact, the worse model performance was found under intense cold front event. According to other authors, the precipitation forecast accuracy depends on the intensity of the precipitation events (Moya-Álvarez et al., 2018).

**Table 3**
Average values of Bias, MAE, RMSE and correlation for 3-h rainfall accumulation.

| | BIAS | MAE | RMSE | r |
|---|---|---|---|---|
| configuration 1 | 0.062831 | 3.895269 | 6.589668 | 0.587587 |
| configuration 2 | −0.504090 | 4.243970 | 7.298406 | 0.495282 |
| configuration 3 | 0.181209 | 4.206904 | 7.073962 | 0.500969 |
| configuration 4 | −0.754269 | 3.666305 | 6.137176 | 0.557184 |
| configuration 5 | −1.666448 | 3.812989 | 6.456754 | 0.557064 |
| configuration 6 | −0.374882 | 4.131263 | 7.041159 | 0.453620 |

**Table 4**
Average values of Bias, MAE, RMSE and correlation for T2m.

| | BIAS | MAE | RMSE | r |
|---|---|---|---|---|
| configuration 1 | −1.108372 | 1.905499 | 2.45724 | 0.869723 |
| configuration 2 | −1.103388 | 1.841778 | 2.387194 | 0.878208 |
| configuration 3 | −1.042808 | 1.802495 | 2.340985 | 0.879837 |
| configuration 4 | −1.107951 | 1.901527 | 2.45491 | 0.869747 |
| configuration 5 | −1.092369 | 1.831298 | 2.378982 | 0.87844 |
| configuration 6 | −1.038473 | 1.795847 | 2.332715 | 0.880667 |

**Table 5**
Average values of Bias, MAE, RMSE and correlation for wind gust.

| | BIAS | MAE | RMSE | r |
|---|---|---|---|---|
| configuration 1 | −4.827238 | 10.802053 | 14.748979 | 0.684739 |
| configuration 2 | −8.289803 | 12.124696 | 16.130221 | 0.67946 |
| Configuration 3 | −5.571593 | 11.338342 | 15.244262 | 0.673237 |
| configuration 4 | −4.886065 | 10.808923 | 14.791971 | 0.68299 |
| configuration 5 | −8.262815 | 12.149721 | 16.18515 | 0.675455 |
| configuration 6 | −5.601049 | 11.349421 | 15.268025 | 0.671952 |

The scatter plot (Fig. 4) shows the correspondence between forecast and observations. An accurate forecast will have points on or near the diagonal. For 3-h rainfall accumulation, most values are below 10 mm/3 h. The plot shows more missed events with forecast values lower than 10 mm/3 h, while observed precipitation was higher than 20 mm/3 h. It is interesting to remark that no model configuration was able to forecast the 50 mm/3 h rainfall accumulation event. The predictability on the precipitation over complex terrain is limited (Hohenegger et al., 2006). This low predictability is due the role of the interactions of the moist flow with orography and the uncertainties in microphysics (Garvert et al., 2005; Colle et al., 2005). The impact of orography on precipitation will be discussed in Section 3.3.

#### 3.1.2. Temperature at 2 m

In contrast with 3-h rainfall accumulation, results obtained for T2m show that configuration 6 obtains the best score. All model configurations underestimate the temperature by 1 °C approximately (bias ≈ −1) and show great correlation with $r$ values higher than 0.86. Temperature underestimation can be justified partly by the method of the soil temperature initialization in the WRF Surface Land Model (SLM) (Cheng and Steenburgh, 2005).

The values obtained in the current work are similar to those obtained by Banks et al. (2016), where the BouLac scheme shows the best performance for T2m.

The scatter plot (Fig. 5) shows, in general, a strong correlation between forecast and observations. The worse correspondences are found when the observed T2m is higher than 15 °C or lower than 0 °C. In the first case (T2m > 15 °C), the model underestimates T2m while in the other case (T2m < 0 °C), the model overestimates it.

#### 3.1.3. Maximum 1-h wind gust

Maximum 1-h wind gust shows the worst verification score. The bias presents significant differences that point to two groups: configurations 2 and 5, and the rest. Configuration 2 and 5 show the largest negative bias; this may be due to the PBL scheme used in both: ACM2. The ACM2 scheme is a hybrid scheme that combines non-local upward closure with local downward closure techniques. Its poor perfor-

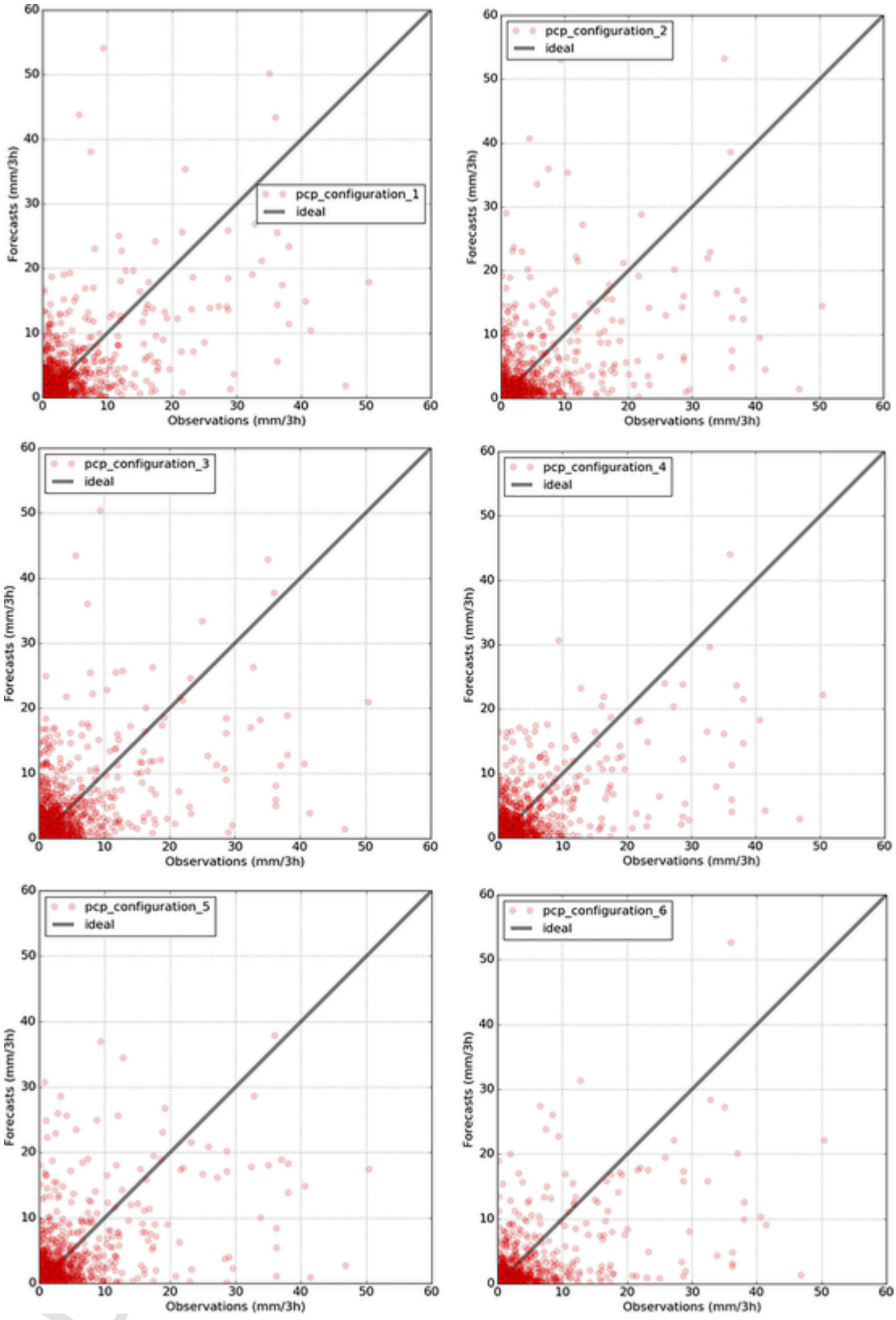


**Fig. 4.** Scatter plot panel for 3-h rainfall accumulation.

mance suggests that some eddies, present on the days tested, were not large enough to be considered non-local, presenting conditions that could be better resolved by the local schemes used in the rest of configurations (MYJ and BouLac).

The MAE and RMSE are higher than 10 km/h. These significant errors can have important consequences in the decision-making process, for instance, in the weather warnings issuance process. Nevertheless, r values are higher than 0.67. Configurations 1 and 4 present the

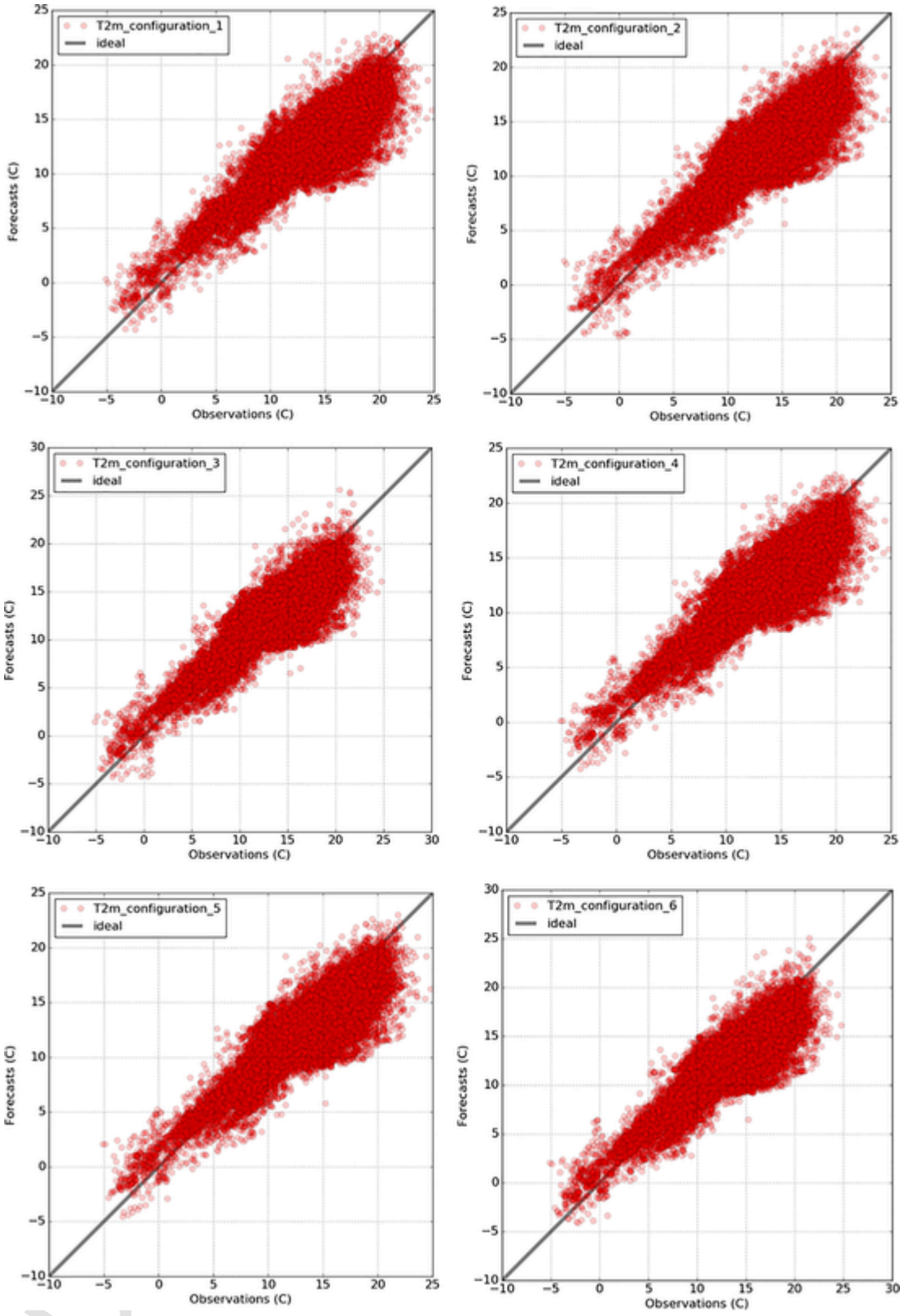


**Fig. 5.** Scatter plot panel for T2m.

best overall results. Both configurations use the MYJ PBL scheme (with MOJ surface layer), confirming the importance of the PBL scheme in wind forecast.

The scatter plot (Fig. 6) shows a systematic model negative bias and remarks the model inability to forecast wind gust >100 km/h. This error can be explained by the inability of the PBL schemes to accurately predict the wind field due to the difficulty to represent the vari-

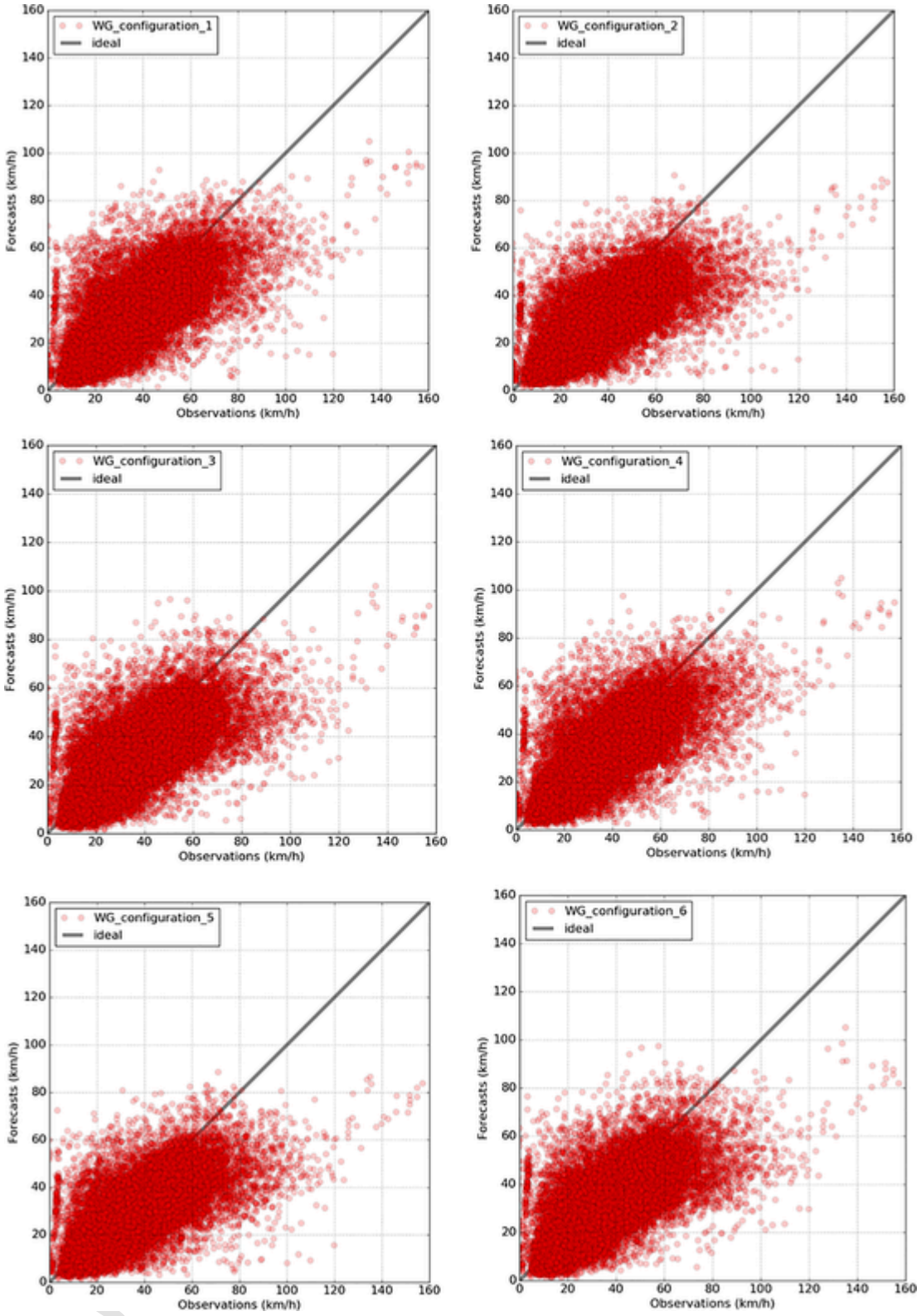


**Fig. 6.** Scatter plot panel for the maximum 1-h wind gust.

ability of the observations (Dandou et al., 2017). This difficulty is particularly relevant in the Canary Islands, given the orographic conditions of the inland stations (Cana et al., 2020).

### *3.2. Lead time dependence*

Figs. 7 to 9 show how the different scores vary with time. In general, all scores change similarly with time and the most relevant differ-

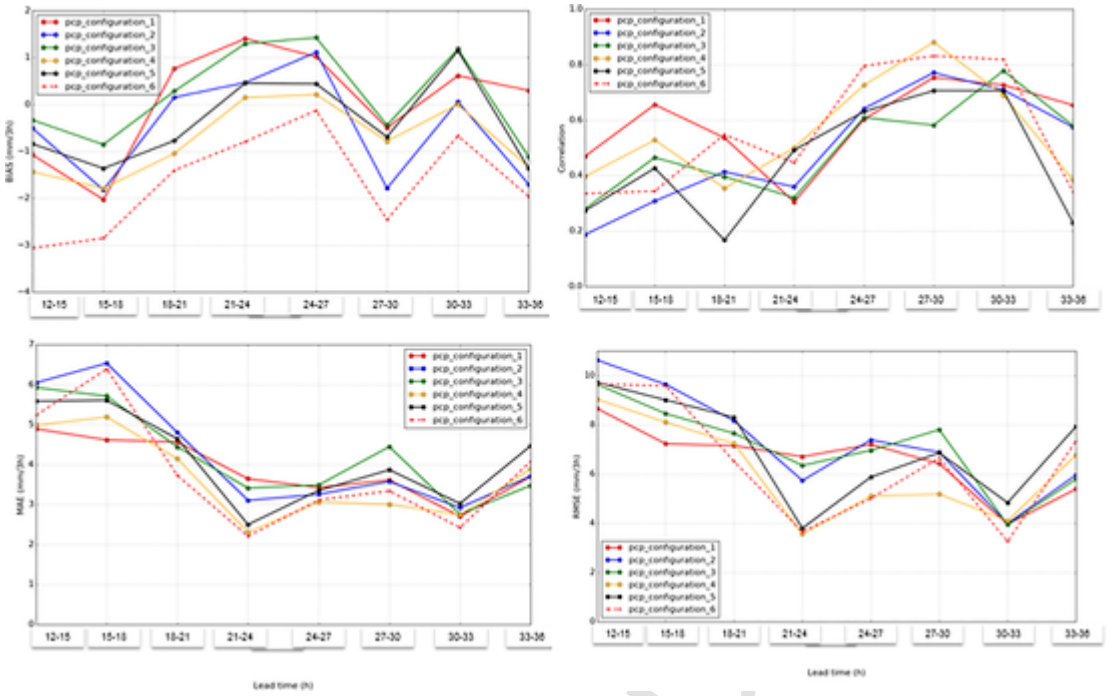


**Fig. 7.** Bias, correlation, MAE and RMSE for 3-h rainfall accumulation.

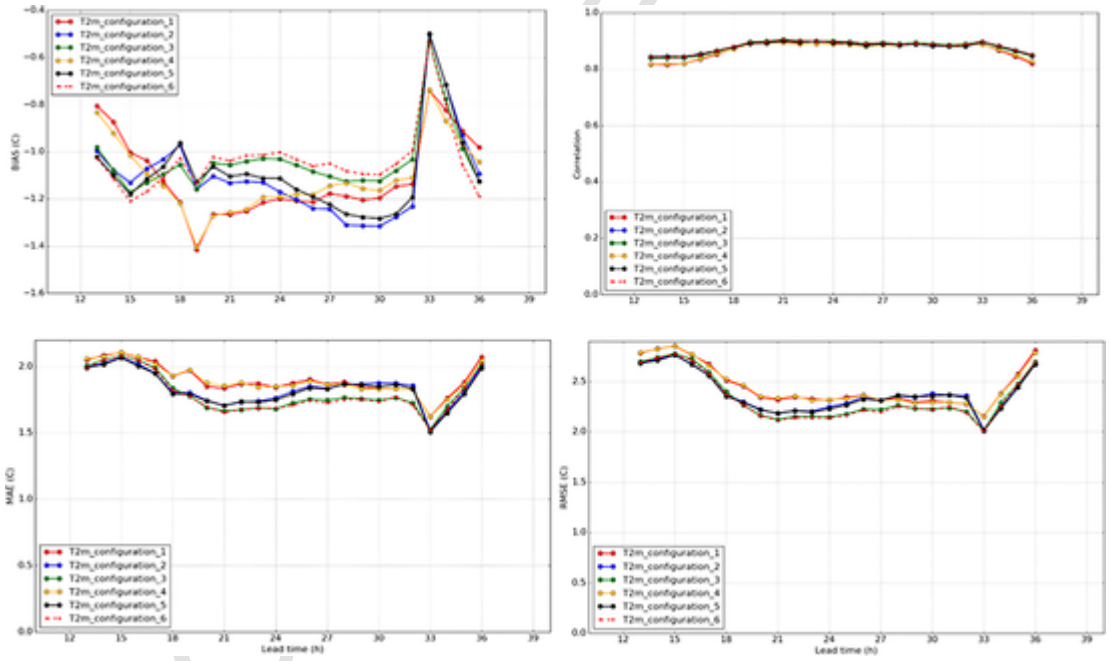


**Fig. 8.** Bias, correlation, MAE and RMSE for T2m.

ence between all model configurations have been found in wind gust bias. As mentioned before, configuration 2 and 5 present the largest negative bias, due to the impact of the PBL scheme used.

In general, the different scores present better results between lead times 18 and 33 h. This suggests that the lead time should be selected carefully when optimizing a WRF configuration in high-resolution models (Jee and Kim, 2017).

a) Precipitation (Fig. 7)

The precipitation correlation increased for all model configuration with time from 0.2 (configuration 2) to higher than 0.8 (configuration 4). The best correlations between observations and forecasts were found during night time and early morning. The precipitation MAE exhibited maxima (close or higher than 5 mm/3 h) during afternoon time (lead time 12–18 h). After, the precipitation MAE decreased from 21 to 33 h of lead time and showed the minima (close to 2 mm/3 h for the configurations 4 and 6) from 21 to 24 h of lead time. The best results were obtained during night time by the fact that the most intense rainfall took place during 12–18 h. As it was seen in the Fig. 4, the fore-

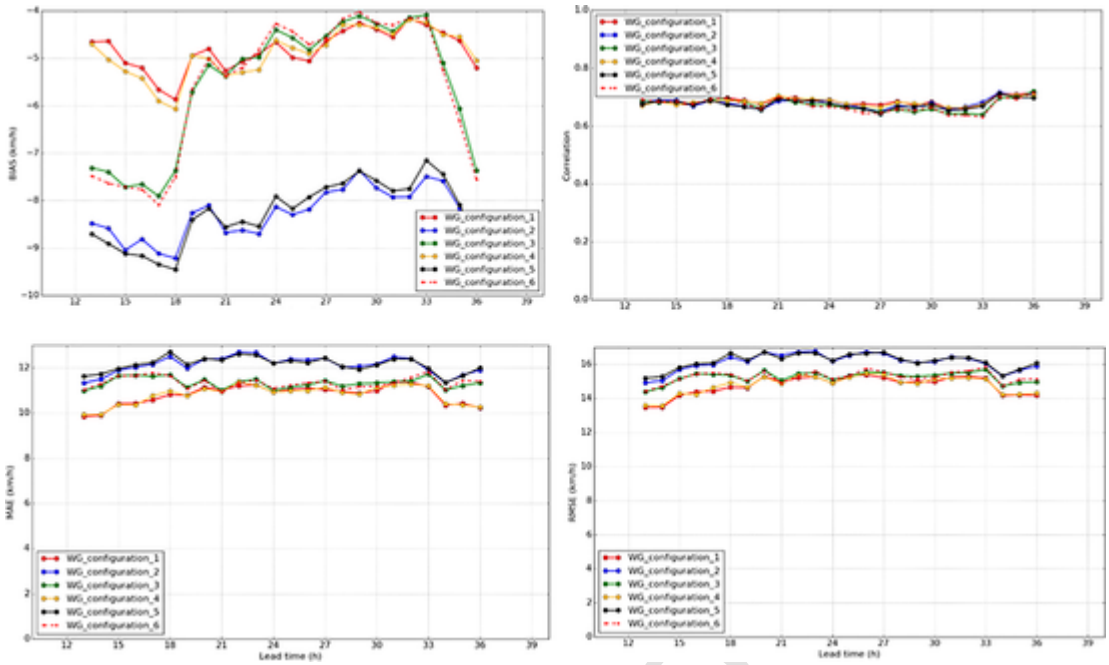


**Fig. 9.** Bias, correlation, MAE and RMSE for the maximum 1-h wind gust.

cast of extreme precipitation is still a challenge. The Boulac-Thompson combination (configuration 6) predicted the lowest precipitation quantities for all lead time.

b) Temperature (Fig. 8)

Fig. 8 shows that all model configurations presented cold temperature bias values around −0.5 °C and − 1.4 °C. The temperature MAE showed three clusters with similar behaviors (configuration 1 and 4, configuration 3 and 6 and configuration 2 and 5) conditioned by the PBL scheme selected. Initially, the temperature MAE was close to 2 °C for all configurations and decreased until 1.5 °C at 33 h. The temperature scores displayed influence of the transition from night to day. All configurations showed more realistic forecast during early morning (33 to 35 h of lead time), while during night time worst results were obtained. It could be related to surface energy fluxes, cloud cover and boundary layer height. As other authors point out (Jousse et al., 2016) inaccurate representation of boundary layer height has a significant implication in the realism of WRF in a stratocumulus region.

c) Wind (Fig. 9)

Fig. 9 shows the behavior of the different model configurations for wind gust throughout the day. Observed mean wind gust displays diurnal variations, with lower speeds during night. All model configurations follow the trends of daily evolution, but configurations 1 and 4 are more realistic. Unlike mean wind gust, the observed maximum wind gust presents higher values during night time with differences between day and night of 20–30 km/h and no model configuration was able to forecast the nocturnal low level jet that forms at night above a temperature inversion. The wind gust correlation was quite similar for all configurations at around 0.67. The lower bias was found for configurations 1 and 4, while configurations 2 and 5 presented larger bias during all period. Configurations 3 and 6 exhibited better result during night time and early morning (from 21 to 33 h).

### 3.3. Location influence

Figs. 10, 11 and 12 show RMSE in observation stations for all model configurations and fields. The main goal of these plots is to find the influence of the location on the forecast accuracy.

Regarding precipitation (Fig. 10), the lowest RMSEs have been obtained in Fuerteventura, Lanzarote and north coasts of Gran Canaria and Tenerife. All configurations present the larger RMSEs in the south and southeast of Tenerife, and in one location of La Gomera. Also, large RMSEs are found in the center of Gran Canaria. The large RMSEs in these locations are due to orographic enhancement of precipitation on the windward slope during extratropical cyclone and cold front events. Despite the convection is explicitly resolved, the orographic precipitation is underestimated; this result is in line with other studies (Hong and Lee, 2009; Eiserloh, 2014; Moya-Álvarez et al., 2019). The forecast of orographic precipitation is a challenge for NWP models as a consequence of the complexity of thermodynamic, cloud microphysics, and dynamic processes in complex terrain (Chow et al., 2013).

In contrast with precipitation, the larger RMSEs for T2m (Fig. 11) are obtained in the east of Fuerteventura, at La Palma airport (east of the island), and at El Hierro airport (northeast of the island). All of them are very close to the sea (less than 500 m) and all of them are located at an altitude lower than 33 m. For these locations, decomposition of RMSE into systematic and unsystematic components evidenced the model's linear (or systematic) error. The cold temperature bias (and the temperature RMSE) oscillated with time between −2.5 °C and − 7.8 °C (and from 3 °C to 8 °C for RMSE) depending on location. However, the worst results were found during days with prevailing intense SW to S winds, with peaks above 100 km/h. Specifically, the largest temperature RMSE was observed at Fuerteventura airport. Under these conditions (strong coast parallel southerly winds), the sea surface temperature (SST) decreases as a reaction to the Coast Low Level Jet (CLLJ) due to upwelling (Fig. 12). The cold current of Portugal–Canary is a potential area of occurrence of CLLJ (Winant et al., 1988). The increase of the temperature RMSE during CLLJ activity enables the unsystematic component and may imply the model impossibility/inability to resolve the phenomenon properly.

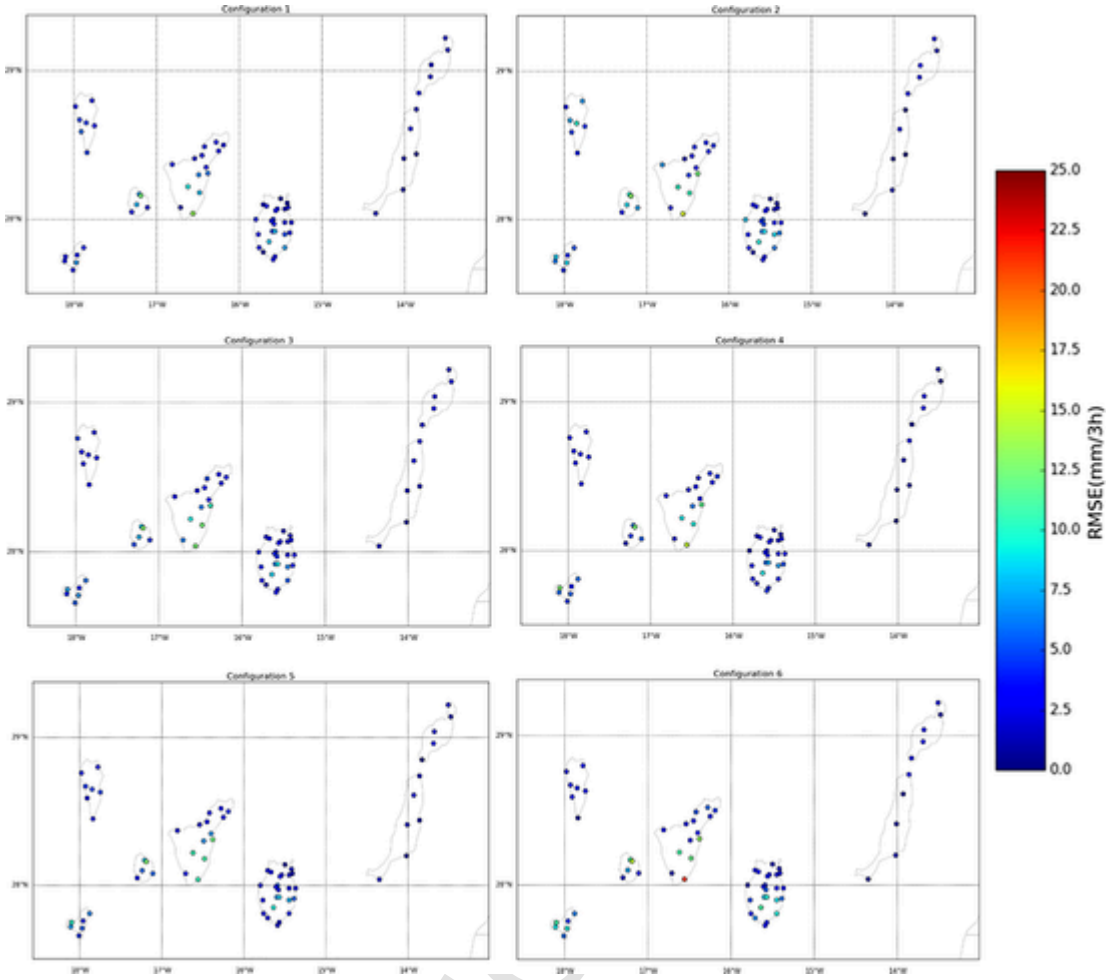


**Fig. 10.** Map of RMSE for 3-h rainfall accumulation by location.

In the case of wind gust (Fig. 13), there are two stations with remarkable large RMSE: Izaña (Tenerife) and Vallehermoso (La Gomera). These errors are related to the intense wind gusts observed in these locations, and the model inability to forecast wind gusts over 100 km/h (as described in Section 3.1.3). The cause of this inability, and the resulting large RMSE, may be related to the complex orography. In these locations, synoptic winds are channeled and terrain-forced flows are produced. Low accuracy wind gust forecast in complex areas is partially justified by the mismatch between real and model topography.

### *3.4. Altitude dependence*

In order to find out the altitude dependence, heatmaps exposing the RMSE as a function of altitude (y-axis) and model configurations (x-axis) are shown in Fig. 14 (rainfall), 15 (T2m) and 16 (wind gust). Each row represents one station except at 0 m, where there are 5 stations. In this case, heatmap shows the average RMSE. For precipitation, 60 out of 68 stations (4 stations at 0 m) were used to make heatmap. The discarded stations did not reach the threshold of 0.2 mm. Red color shows high RMSE, whereas blue color shows low RMSE.

The precipitation RMSE increased with the altitude from 0 to 12 mm/3 h (Fig. 14). However, the largest precipitation RMSE (between 15 and 24 mm/3 h) were found below 170 m. These high values of precipitation RMSE at low altitude were due to a singular maximum peak (44.6 mm/3 h accumulated in an hour) at Tenerife Sur airport under low pressure system and cold front conditions. Although the configuration model 5 reproduced better the peak, the difference between observation and forecast was 20 mm/3 h. Finally, we must consider that, in locations characterized by shallow cumulus regimes, such as the Canary Islands, the existing PBL parametrizations in the WRF model are unable to produce fully accurate results (Huang et al., 2013; Carrillo et al., 2016; Jousse et al., 2016; Gunwani and Mohan, 2017; Cana et al., 2020).

T2m does not show a direct relationship between altitude and RMSE. However, the worst results, as explained before (Fig. 15), are found at low altitudes. Analyzing different strata, in average the highest T2m RMSE (from 2 to 4.2 °C) was found at 0–50 m, highly influenced by the larger RMSE due to location influence. The strata at 50–500, 500–1000, and 1000–1500 m presented similar T2m RMSE (in average between 1.5 and 2.5 °C). Nevertheless, station at higher than 1500 m presented great variability of T2m RMSE. In high mountain areas (altitude above 1500 m) larger T2m RMSE were obtained during days with great thermal oscillation with minimal temperatures of −5 °C and maximum temperatures of 12 °C.

Regarding wind gust, RMSE increase with altitude in all cases (Fig. 16). The increase of RMSE with altitude is related to sub-grid terrain features and its impact on the wind gust (see Section 3.3).

## 4. Conclusions

Sensitivity analysis can be used to determine optimum WRF model configurations. However, the best configuration depends on location and meteorological conditions. In this research, a comprehensive sensitivity analysis has been carried out in the Canary Islands. Due to the impact on the socio-economic activities, the analysis has been fo-

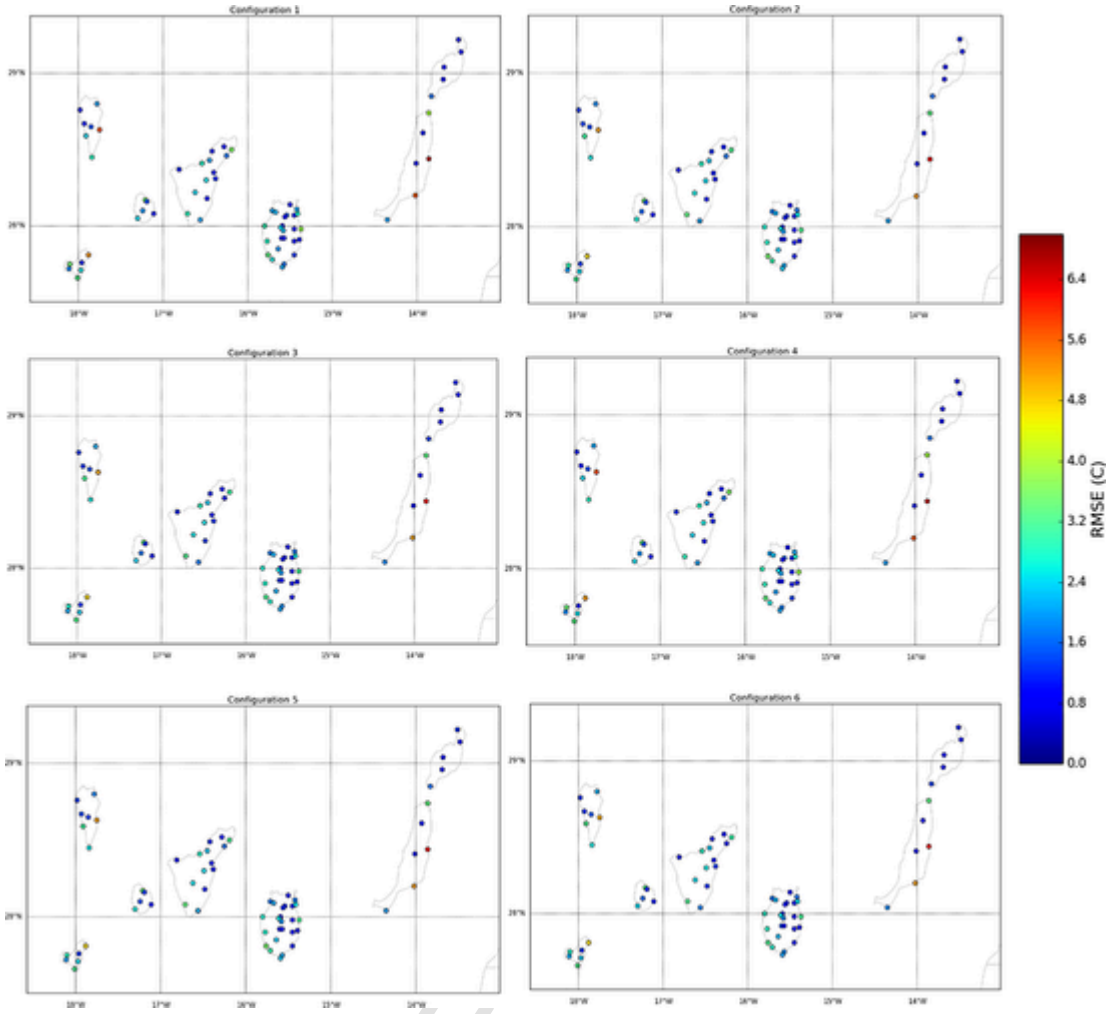


**Fig. 11.** Map of RMSE for T2m by location.

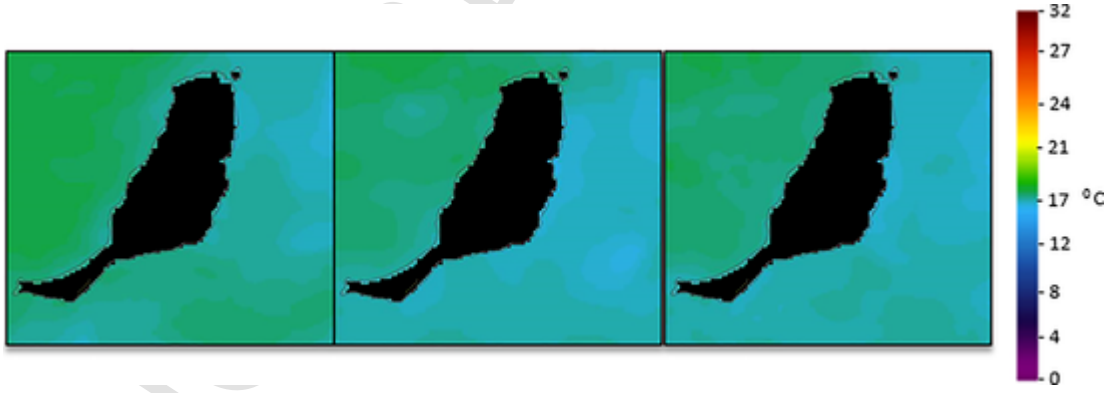


**Fig. 12.** Sea Surface Temperature around Fuerteventura from the Group for High Resolution Sea Surface Temperature (GHRSST). Under upwelling conditions (February 26 and 27, center and right image) SST is lower (blue color) on the east coast than under trade wind conditions (green color) (February 16, left image) (https://worldview.earthdata.nasa.gov/ SST). (For interpretation of the references to color in this figure legend, the reader is referred to the web version of this article.)

cused on T2m, wind gust and 3-h rainfall accumulation. Subsequently, the most relevant conclusions are summarized:

- This research allowed discarding inappropriate WRF model configurations. The discarded configurations were the combinations of YSU, MYNN2 PBL schemes with Kessler, Goddard and Morrison 2-Moment MP schemes.
- Regarding the 3-h rainfall accumulation on the Canary Islands, the PBL scheme selected had a greater impact than the MP scheme used. The MYJ PBL scheme reached the best performance for precipitation. The ability of the model configurations to forecast precipitation was influenced by the daytime.
- The BouLac-Thompson combination presented the best results for T2m.

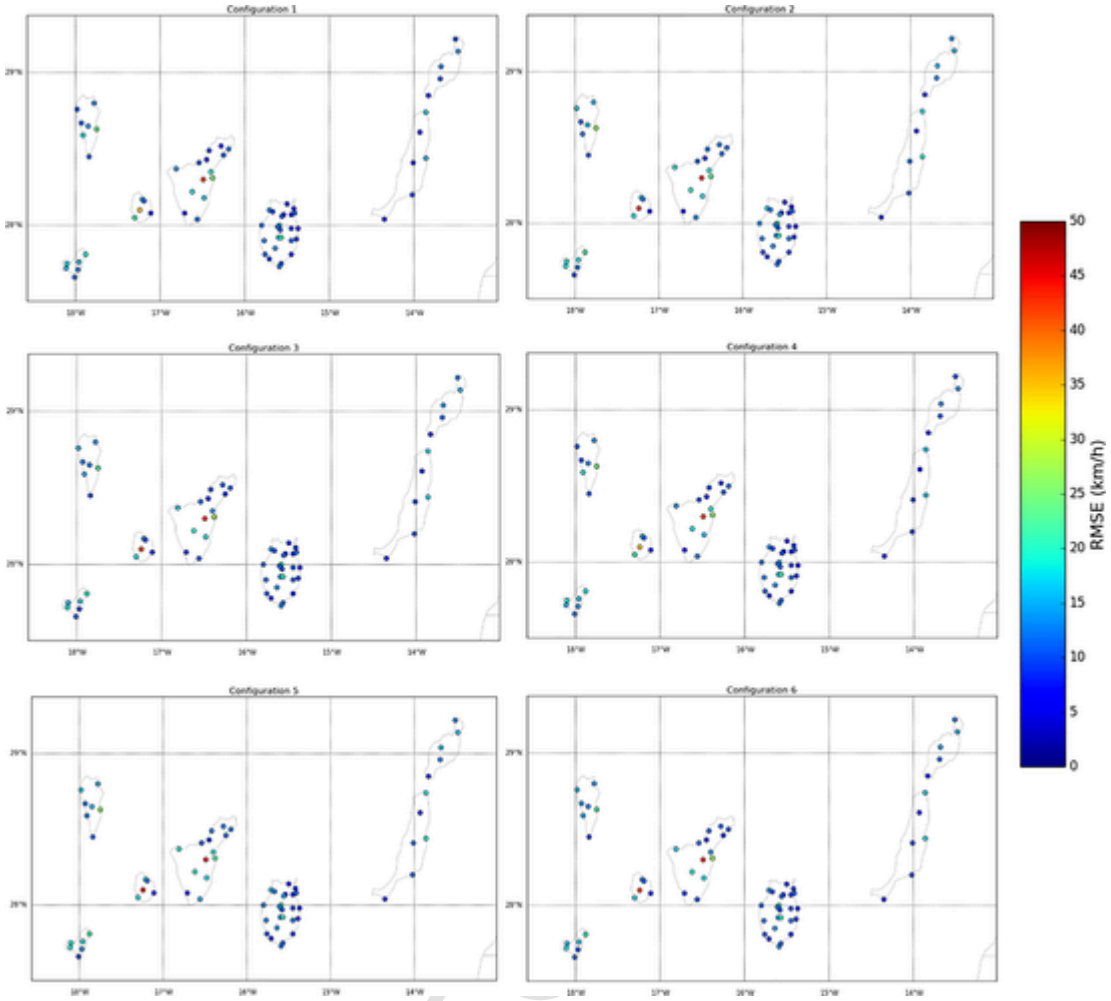


**Fig. 13.** Map of RMSE for maximum 1-h wind gust by location.

- The combination of MYJ-WSM6 showed the best results for the maximum 1-h wind gust. All model configurations followed the trends of daily evolution for mean wind gust. However, none was able to forecast nocturnal low level jet. Although the MYJ PBL scheme presented more stable results for wind gust with time, the Boulac PBL scheme exhibited better results during night time and early morning.
- All fields presented better results between lead time 18 and 33 h.
- The influence of the location was proved. The worst overall results were obtained in complex terrain areas. Worst T2m results arose in the land-sea transition zones on the eastern coasts of the islands. Also, for 3-h rainfall accumulation and maximum 1-h wind gust, the forecast error increased with altitude.

There was a systematic wind speed underestimation in all configurations. This underestimation suggests that, to obtain better results, either other configurations should be tested, or post processing techniques should be explored. The results obtained in this article show the difficulty to obtain accurate forecasts in complex orography areas. Therefore, in these areas, resources must be invested to test the models and achieve an optimal configuration. The results reached in this study can be taken as the basis for future WRF configurations in operational mode within AEMET for the Canary Islands domain.

## Author statement

The paper entitled "Sensitivity analysis of the WRF Model: Assessment of performance in high resolution simulations in complex terrain in the Canary Islands" was carried out by the authors David Suárez-Molina, Sergio Fernández-González, Gustavo Montero, Albert Oliver and Juan Carlos Suárez González. In the following lines, the contribution of each author will be detailed:

David Suárez-Molina: He is the main contributor to this paper, being the responsible of the conceptualization, design of the methodology, obtaining results, and writing.

Sergio Fernández-González has contributed in the redaction of the paper, and supervising the research activity.

Gustavo Montero and Albert Oliver have contributed in the research design, and collaborated in the redaction of the paper.

Juan Carlos Suárez González has helped with the software, data curation and formal analysis.

## Declaration of Competing Interest

The authors claim that there is no conflict of interest, nor any funding source that intercedes with the free publication of results obtained in this research.

## Acknowledgements

Observational data are provided by the State Meteorological Agency of Spain (AEMET). The authors are grateful to the Weather Forecast Research Team for developing "Verif" software. Special thanks go to the

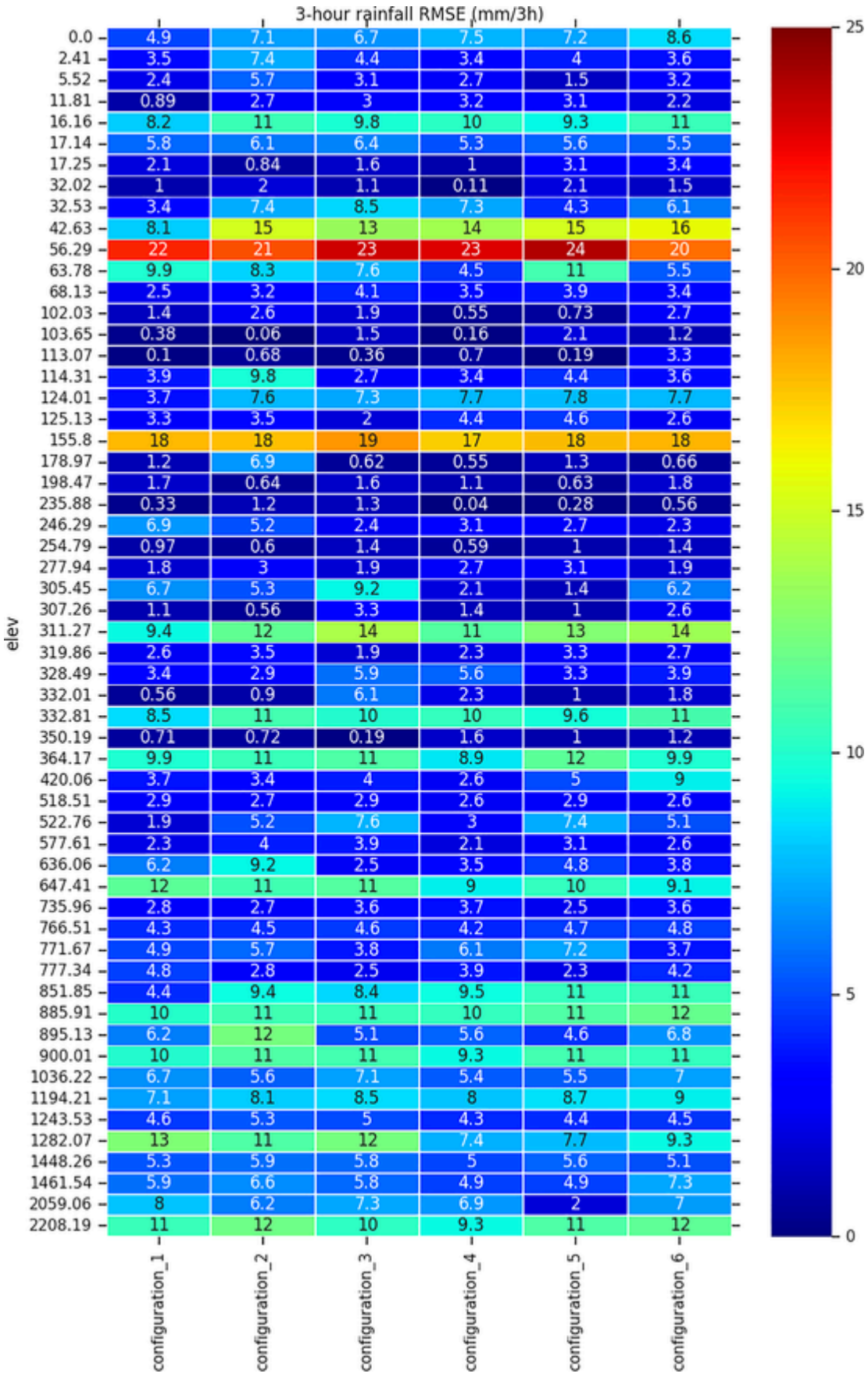
3-hour rainfall RMSE (mm/3h)
elev
0.0 4.9 7.1 6.7 7.5 7.2 8.6
2.41 3.5 7.4 4.4 3.4 4 3.6
5.52 2.4 5.7 3.1 2.7 1.5 3.2
11.81 0.89 2.7 3 3.2 3.1 2.2
16.16 8.2 11 9.8 10 9.3 11
17.14 5.8 6.1 6.4 5.3 5.6 5.5
17.25 2.1 0.84 1.6 1 3.1 3.4
32.02 1 2 1.1 0.11 2.1 1.5
32.53 3.4 7.4 8.5 7.3 4.3 6.1
42.63 8.1 15 13 14 15 16
56.29 22 21 23 23 24 20
63.78 9.9 8.3 7.6 4.5 11 5.5
68.13 2.5 3.2 4.1 3.5 3.9 3.4
102.03 1.4 2.6 1.9 0.55 0.73 2.7
103.65 0.38 0.06 1.5 0.16 2.1 1.2
113.07 0.1 0.68 0.36 0.7 0.19 3.3
114.31 3.9 9.8 2.7 3.4 4.4 3.6
124.01 3.7 7.6 7.3 7.7 7.8 7.7
125.13 3.3 3.5 2 4.4 4.6 2.6
155.8 18 18 19 17 18 18
178.97 1.2 6.9 0.62 0.55 1.3 0.66
198.47 1.7 0.64 1.6 1.1 0.63 1.8
235.88 0.33 1.2 1.3 0.04 0.28 0.56
246.29 6.9 5.2 2.4 3.1 2.7 2.3
254.79 0.97 0.6 1.4 0.59 1 1.4
277.94 1.8 3 1.9 2.7 3.1 1.9
305.45 6.7 5.3 9.2 2.1 1.4 6.2
307.26 1.1 0.56 3.3 1.4 1 2.6
311.27 9.4 12 14 11 13 14
319.86 2.6 3.5 1.9 2.3 3.3 2.7
328.49 3.4 2.9 5.9 5.6 3.3 3.9
332.01 0.56 0.9 6.1 2.3 1 1.8
332.81 8.5 11 10 10 9.6 11
350.19 0.71 0.72 0.19 1.6 1 1.2
364.17 9.9 11 11 8.9 12 9.9
420.06 3.7 3.4 4 2.6 5 9
518.51 2.9 2.7 2.9 2.6 2.9 2.6
522.76 1.9 5.2 7.6 3 7.4 5.1
577.61 2.3 4 3.9 2.1 3.1 2.6
636.06 6.2 9.2 2.5 3.5 4.8 3.8
647.41 12 11 11 9 10 9.1
735.96 2.8 2.7 3.6 3.7 2.5 3.6
766.51 4.3 4.5 4.6 4.2 4.7 4.8
771.67 4.9 5.7 3.8 6.1 7.2 3.7
777.34 4.8 2.8 2.5 3.9 2.3 4.2
851.85 4.4 9.4 8.4 9.5 11 11
885.91 10 11 11 10 11 12
895.13 6.2 12 5.1 5.6 4.6 6.8
900.01 10 11 11 9.3 11 11
1036.22 6.7 5.6 7.1 5.4 5.5 7
1194.21 7.1 8.1 8.5 8 8.7 9
1243.53 4.6 5.3 5 4.3 4.4 4.5
1282.07 13 11 12 7.4 7.7 9.3
1448.26 5.3 5.9 5.8 5 5.6 5.1
1461.54 5.9 6.6 5.8 4.9 4.9 7.3
2059.06 8 6.2 7.3 6.9 2 7
2208.19 11 12 10 9.3 11 12
configuration_1
configuration_2
configuration_3
configuration_4
configuration_5
configuration_6
25
20
15
10
5
0

**Fig. 14.** Heatmap of RMSE for 3-h rainfall by altitude and configuration.

SAFEFLIGHT (CGL2016-78702-C2-1-R and CGL2016-78702-C2-2-R) and UE ERA-NET Plus NEWA (PCIN2016-080) projects.

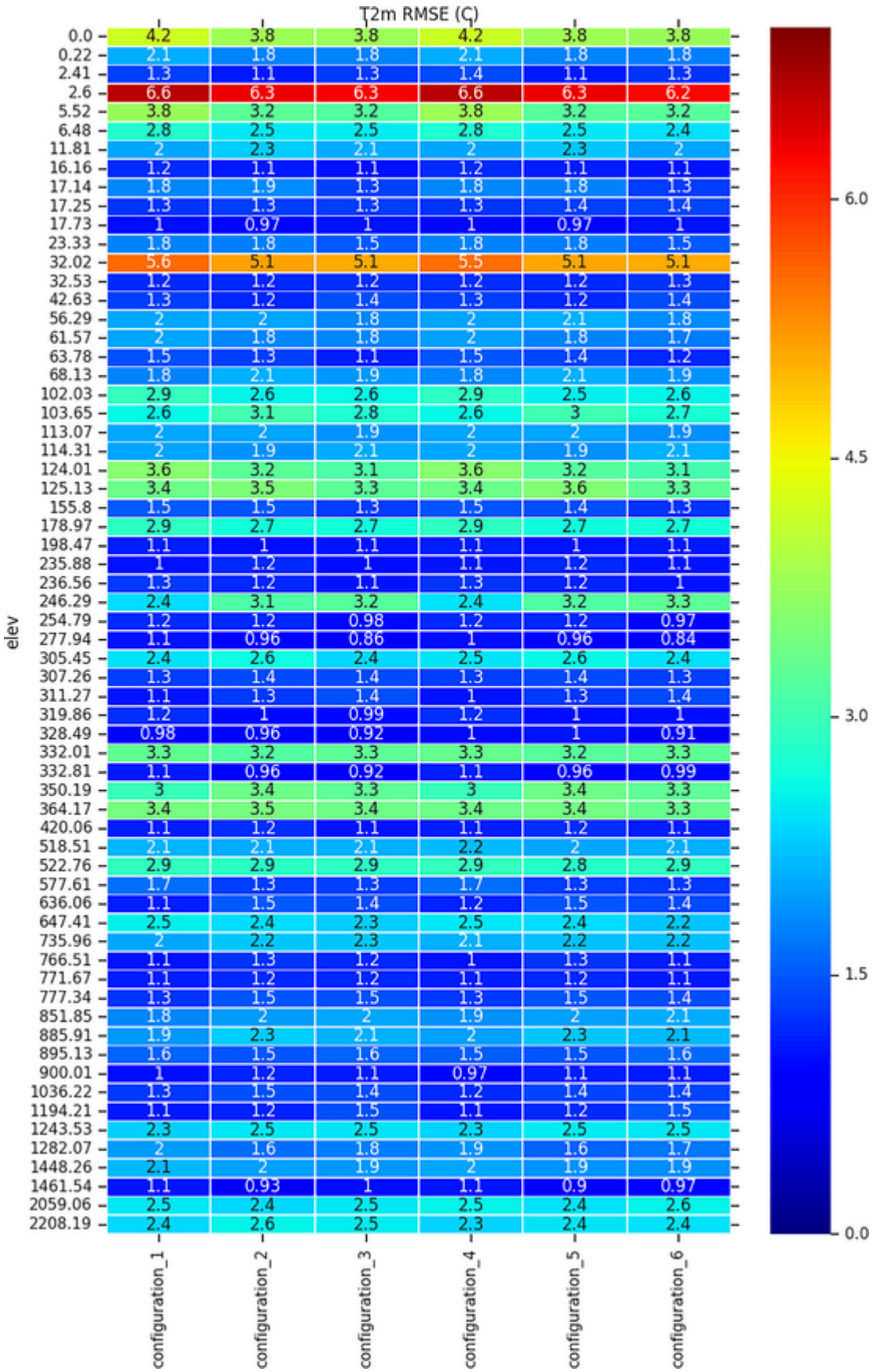


**Fig. 15.** Heatmap of RMSE for T2m by altitude and configuration.

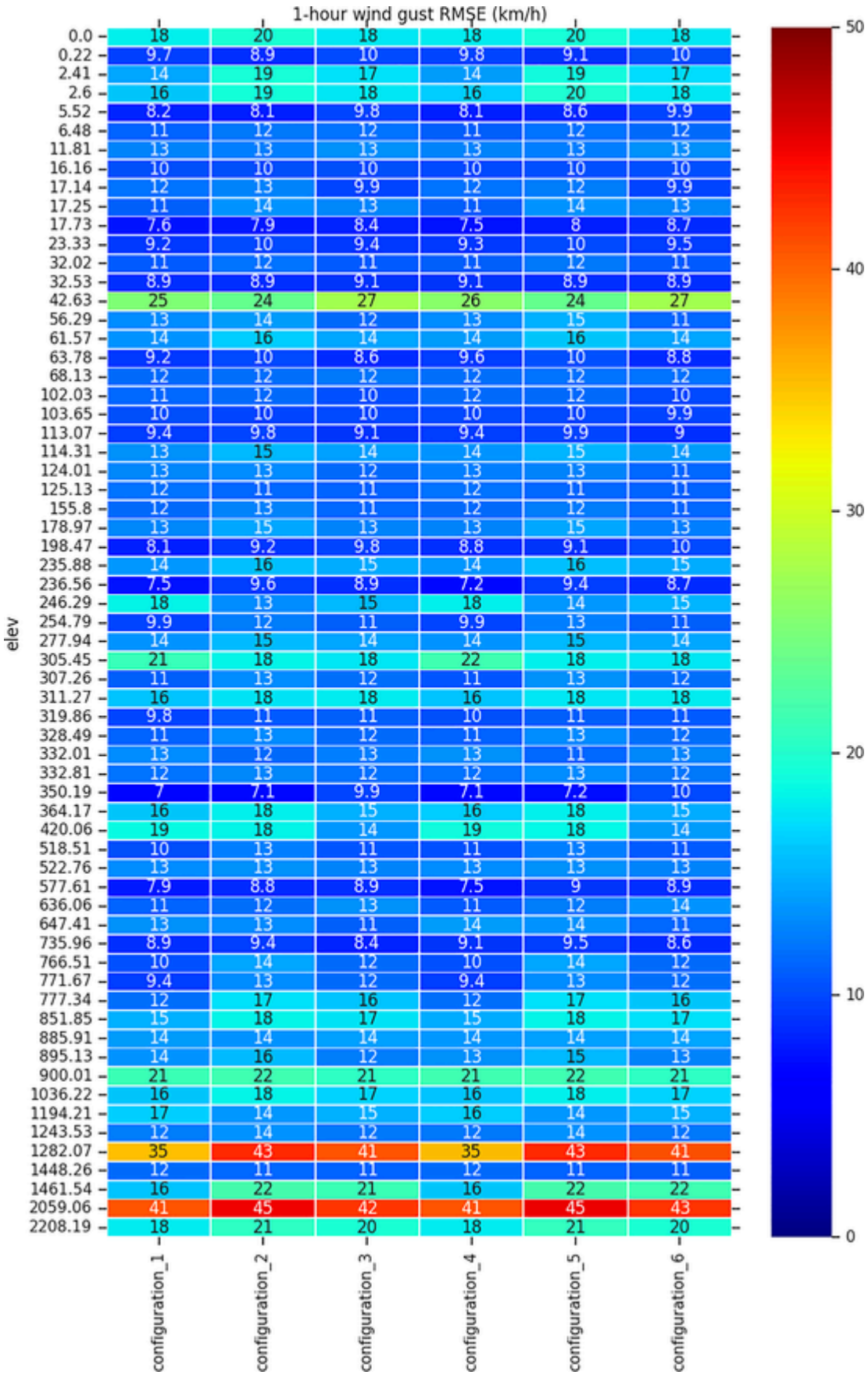
1-hour wind gust RMSE (km/h)
elev
0.0 18 20 18 18 20 18
0.22 9.7 8.9 10 9.8 9.1 10
2.41 14 19 17 14 19 17
2.6 16 19 18 16 20 18
5.52 8.2 8.1 9.8 8.1 8.6 9.9
6.48 11 12 12 11 12 12
11.81 13 13 13 13 13 13
16.16 10 10 10 10 10 10
17.14 12 13 9.9 12 12 9.9
17.25 11 14 13 11 14 13
17.73 7.6 7.9 8.4 7.5 8 8.7
23.33 9.2 10 9.4 9.3 10 9.5
32.02 11 12 11 11 12 11
32.53 8.9 8.9 9.1 9.1 8.9 8.9
42.63 25 24 27 26 24 27
56.29 13 14 12 13 15 11
61.57 14 16 14 14 16 14
63.78 9.2 10 8.6 9.6 10 8.8
68.13 12 12 12 12 12 12
102.03 11 12 10 12 12 10
103.65 10 10 10 10 10 9.9
113.07 9.4 9.8 9.1 9.4 9.9 9
114.31 13 15 14 14 15 14
124.01 13 13 12 13 13 11
125.13 12 11 11 12 11 11
155.8 12 13 11 12 12 11
178.97 13 15 13 13 15 13
198.47 8.1 9.2 9.8 8.8 9.1 10
235.88 14 16 15 14 16 15
236.56 7.5 9.6 8.9 7.2 9.4 8.7
246.29 18 13 15 18 14 15
254.79 9.9 12 11 9.9 13 11
277.94 14 15 14 14 15 14
305.45 21 18 18 22 18 18
307.26 11 13 12 11 13 12
311.27 16 18 18 16 18 18
319.86 9.8 11 11 10 11 11
328.49 11 13 12 11 13 12
332.01 13 12 13 13 11 13
332.81 12 13 12 12 13 12
350.19 7 7.1 9.9 7.1 7.2 10
364.17 16 18 15 16 18 15
420.06 19 18 14 19 18 14
518.51 10 13 11 11 13 11
522.76 13 13 13 13 13 13
577.61 7.9 8.8 8.9 7.5 9 8.9
636.06 11 12 13 11 12 14
647.41 13 13 11 14 14 11
735.96 8.9 9.4 8.4 9.1 9.5 8.6
766.51 10 14 12 10 14 12
771.67 9.4 13 12 9.4 13 12
777.34 12 17 16 12 17 16
851.85 15 18 17 15 18 17
885.91 14 14 14 14 14 14
895.13 14 16 12 13 15 13
900.01 21 22 21 21 22 21
1036.22 16 18 17 16 18 17
1194.21 17 14 15 16 14 15
1243.53 12 14 12 12 14 12
1282.07 35 43 41 35 43 41
1448.26 12 11 11 12 11 11
1461.54 16 22 21 16 22 22
2059.06 41 45 42 41 45 43
2208.19 18 21 20 18 21 20
configuration_1
configuration_2
configuration_3
configuration_4
configuration_5
configuration_6
50
40
30
20
10
0

**Fig. 16.** Heatmap of RMSE for wind gust by altitude and configuration.

## References


Eiserloh, Arthur John, 2014. WRF-Model Data Assimilation Studies of Landfalling Atmospheric Rivers and Orographic Precipitation Over Northern California. Master's Theses. 4461. doi:10.31979/etd.5wgq-5vkc. https://scholarworks.sjsu.edu/etd_theses/4461.

Anderson, M C, Norman, J M, Diak, G R, Kustas, W P, Mecikalski, J R, 2011. A two-source time integrated model for estimating surface fluxes using thermal infrared remote sensing. Remote Sens. Environ. 60 (2), 195–216. doi:10.1016/s0034-4257(96)00215-5.

Banks, R F, Tiana-Alsina, J, Baldasano, J M, Rocadenbosch, F, Papayannis, A, Solomos, S, Tzanis, C G, 2016. Sensitivity of boundary-layer variables to PBL schemes in the WRF model based on surface meteorological observations, lidar, and radiosondes during the HygrA-CD campaign. Atmos. Res. 176–177, 185–201. doi:10.1016/j.atmosres.2016.02.024.

Biswas, M K, Bernardet, L, Abarca, S, Ginis, I, Grell, E, Kalina, E, Zhang, Z, 2018. Hurricane Weather Research and Forecasting (HWRF) Model: 2017 Scientific Documentation (No. NCAR/TN-544+STR). doi:10.5065/D6MK6BPR.

Borge, R, Alexandrov, V, del Vas, J J, Lumbreras, J, Rodríguez, E, 2008. A comprehensive sensitivity analysis of the WRF model for air quality applications over the Iberian Peninsula. Atmos. Environ. 42 (37), 8560–8574. doi:10.1016/j.atmosenv.2008.08.032.

Bossioli, E, Tombrou, M, Dandou, A, Athanasopoulou, E, Varotsos, K V, 2009. The role of planetary boundary-layer parameterizations in the air quality of an urban area with complex topography. Bound. Layer Meteorol. 131, 53–72. doi:10.1007/s10546-009-9349-7.

Bougeault, P, Lacarrere, P, 1989. Parameterization of orography-induced turbulence in a mesobeta--scale model. Mon. Weather Rev. 117 (8), 1872–1890. doi:10.1175/1520-0493(1989)117<1872:pooiti>2.0.co;2.

Callado, A., Escribà, P., Gil, D., Compte., M, Martínez, M., González, S., Quintero, D., García-Moya, J.A., 2019. AEMET-γSREPS en operaciones. Sexto Simposio Nacional de Predicción, Memorial Antonio Mestre. http://hdl.handle.net/20.500.11765/10995.

Cana, L, Grisolía-Santos, D, Hernández-Guerra, A, 2020. A Numerical Study of a Sea Breeze at Fuerteventura Island, Canary Islands, Spain. Bound.-Layer Meteorol. 175 (2), 277–296. doi:10.1007/s10546-020-00506-z.

Carrillo, J, Guerra, J C, Cuevas, E, Barrancos, J, 2016. Characterization of the marine boundary layer and the trade-wind inversion over the sub-tropical North Atlantic. Boundary-Layer Meteorol. 158, 311–330. doi:10.1007/s10546-015-0081-1.

Chen, F, Dudhia, J, 2001. Coupling an advanced land surface–hydrology model with the Penn State–NCAR MM5 modeling system. Part I: model implementation and sensitivity. Mon. Weather Rev. 129 (4), 569–585. doi:10.1175/1520-0493(2001)129<0569:caalsh>2.0.co;2.

Cheng, W Y Y, Steenburgh, W J, 2005. Evaluation of Surface Sensible Weather forecasts by the WRF and the Eta Models over the Western United States. Weather Forecasting 20, 812–821. doi:10.1175/WAF885.1.

Chow, F K, De Wekker, S F J, Snyder, B J, 2013. Mountain Weather Research and Forecasting. Springer Atmospheric Sciences. doi:10.1007/978-94-007-4098-3.

Colle, B A, Garvert, M F, Wolfe, J B, Mass, C F, Woods, C P, 2005. The 13–14 December 2001 IMPROVE-2 event. Part III: simulated microphysical budgets and sensitivity studies. J. Atmos. Sci. 62 (10), 3535–3558. doi:10.1175/jas3552.1.

Dandou, A, Tombrou, M, Kalogiros, J, Bossioli, E, Biskos, G, Mihalopoulos, N, Coe, H, 2017. Investigation of turbulence parametrization schemes with reference to the atmospheric boundary layer over the Aegean Sea during etesian winds. Boundary-Layer Meteorol. 164, 303–329. doi:10.1007/s10546-017-0255-0.

Dorta, P, 2007. Catálogo de riesgos climáticos en Canarias: Amenazas y vulnerabilidad. Geographicalia 133–160, 51 ISSN 0210-8380, N° 51. doi:10.26754/ojs_geoph/geoph.2007511118.

Evans, J P, Ekström, M, Ji, F, 2012. Evaluating the performance of a WRF physics ensemble over South-East Australia. Clim. Dynam. 39 (6), 1241–1258. doi:10.1007/s00382-011-1244-5.

Fernández-González, S, Valero, F, Sánchez, J L, Gascón, E, López, L, García-Ortega, E, Merino, A, 2015. Numerical simulations of snowfall events: Sensitivity analysis of physical parameterizations. J. Geophys. Res.-Atmos. 120 (19), 10–130. doi:10.1002/2015jd023793.

Fernández-González, S, Martín, M L, Merino, A, Sánchez, J L, Valero, F, 2017. Uncertainty quantification and predictability of wind speed over the Iberian Peninsula. J. Geophys. Res.-Atmos. 122 (7), 3877–3890. doi:10.1002/2017jd026533.

Fernández-González, S, Martín, M L, García-Ortega, E, Merino, A, Lorenzana, J, Sánchez, J L, Rodrigo, J S, 2018. Sensitivity analysis of the WRF model: wind-resource assessment for complex terrain. J. Appl. Meteorol. Clim. 57 (3), 733–753. doi:10.1175/jamc-d-17-0121.1.

García-Ortega, E, Lorenzana, J, Merino, A, Fernández-González, S, López, L, Sánchez, J L, 2017. Performance of multi-physics ensembles in convective precipitation events over northeastern Spain. Atmos. Res. 190, 55–67. doi:10.1016/j.atmosres.2017.02.009.

Garvert, M F, Woods, C P, Colle, B A, Mass, C F, Hobbs, P V, Stoelinga, M T, Wolfe, J B, 2005. The 13–14 December 2001 IMPROVE-2 event. Part II: Comparisons of MM5 model simulations of clouds and precipitation with observations. J. Atmos. Sci. 62 (10), 3520–3534.

González Rocha, S, Juárez-Pérez, F, Aguilar-Meléndez, A, Cristobalsalas, A, Calderón-Ramón, C, Escalante-Martínez, J, Baldasano, J, 2017. Planet Boundary Layer Parameterization in Weather Research and forecasting (WRFv3.5): Assessment of Performance in High Spatial Resolution Simulations in complex Topography of Mexico. Computacion y Sistemas. 21, 35–44. doi:10.13053/CyS-21-1-2581.

Gunwani, P, Mohan, M, 2017. Sensitivity of WRF model estimates to various PBL parameterizations in different climatic zones over India. Atmos. Res. 194, 43–65. doi:10.1016/j.atmosres.2017.04.026.

Hamill, T M, 2014. Performance of Operational Model Precipitation Forecast Guidance during the 2013 Colorado Front-Range Floods. Mon. Weather Rev. 142, 2609–2618. doi:10.1175/MWR-D-14-00007.1.

Hohenegger, C, Lüthi, D, Schär, C, 2006. Predictability mysteries in cloud-resolving models. Mon. Weather. Rev. 134 (8), 2095–2107. doi:10.1175/mwr3176.1.

Hong, Song-You, Lee, Ji-Woo, 2009. Assessment of the WRF model in reproducing a flash-flood heavy rainfall event over Korea. Atmos. Res. 93 (4), 818–831. doi:10.1016/j.atmosres.2009.03.015.

Hong, S Y, Lim, J O J, 2006. The WRF single-moment 6-class microphysics scheme (WSM6). Asia Pac. J. Atmos. Sci. 42 (2), 129–151.

Hong, S Y, Noh, Y, Dudhia, J, 2006. A new vertical diffusion package with an explicit treatment of entrainment processes. Mon. Weather Rev. 134 (9), 2318–2341. doi:10.1175/mwr3199.1.

Hsiao, L, Chen, D, Kuo, Y, Guo, Y, Yeh, T, Hong, J, Fong, C, Lee, C, 2012. Application of WRF 3DVAR to Operational Typhoon Prediction in Taiwan: Impact of Outer Loop and Partial Cycling Approaches. Weather Forecasting 27, 1249–1263. doi:10.1175/WAF-D-11-00131.1.

Huang, H-Y, Hall, A, Teixeira, J, 2013. Evaluation of the WRF PBL parameterizations for marine boundary layer clouds: cumulus and stratocumulus. Mon. Weather Rev. 141, 2265–2271. doi:10.1175/mwr-d-12-00292.1.

Iacono, M J, Delamere, J S, Mlawer, E J, Shephard, M W, Clough, S A, Collins, W D, 2008. Radiative forcing by long-lived greenhouse gases: Calculations with the AER radiative transfer models. J. Geophys. Res.-Atmos. 113, D13. doi:10.1029/2008jd009944.

Janjic, Z I, 1994. The step-mountain eta coordinate model: further developments of the convection, viscous sublayer and turbulence closure schemes. Mon. Weather Rev. 122, 927–945. doi:10.1175/1520-0493(1994)122<0927:tsmecm>2.0.co;2.

Jee, J B, Kim, S, 2017. Sensitivity study on high-resolution WRF precipitation forecast for a heavy rainfall event. Atmosphere 8 (6), 96. doi:10.3390/atmos8060096.

Jiménez, P A, González-Rouco, J F, García-Bustamante, E, Navarro, J, Montávez, J P, de Arellano, J V-G, Dudhia, J, Muñoz-Roldan, A, 2010. Surface Wind Regionalization over Complex Terrain: Evaluation and Analysis of a High-Resolution WRF simulation. J. Appl. Meteorol. Clim. 49, 268–287. doi:10.1175/2009JAMC2175.1.

Johnson, A, Wang, X, 2012. Verification and calibration of neighborhood and object-based probabilistic precipitation forecasts from a multimodel convection-allowing ensemble. Mon. Weather Rev. 140 (9), 3054–3077. doi:10.1175/mwr-d-11-00356.1.

Jorba, O, Marrero, C, Cuevas, E, Baldasano, J M, 2015. Numerical Modelling of the Extratropical storm Delta over Canary Islands: Importance of High Resolution. In: Klapp, J, Ruíz, Chavarría G, Medina, Ovando A, López, Villa A, Sigalotti, L (Eds.), Selected Topics of Computational and Experimental Fluid Mechanics. Environmental Science and Engineering. Springer, Cham. doi:10.1007/978-3-319-11487-3_7.

Jousse, A, Hall, A, Sun, F, Teixeira, J, 2016. Causes of WRF surface energy fluxes biases in a stratocumulus region. Clim. Dyn. 46, 571–584. doi:10.1007/s00382-015-2599-9.

Kain, J S, 2004. The Kain–Fritsch convective parameterization: an update. J. Appl. Meteorol. 43 (1), 170–181. doi:10.1175/1520-0450(2004)043<0170:tkcpau>2.0.co;2.

Kessler, E, 1969. On the distribution and continuity of water substance in atmospheric circulations. In: On the Distribution and Continuity of Water Substance in Atmospheric Circulations. American Meteorological Society, Boston, MA, pp. 1–84. doi:10.1007/978-1-935704-36-2_1.

Marrero, C, Jorba, O, Cuevas, E, Baldasano, J M, 2008. Sensitivity study of surface wind flow of a limited area model simulating the extratropical storm Delta affecting the Canary Islands. Adv. Sci. Res. 2, 151–157. doi:10.5194/asr-2-151-2008.

Martilli, A, Clappier, A, Rotach, M W, 2002. An urban surface exchange parameterisation for mesoscale models. Boundary-layer Meteorol. 104 (2), 261–304. doi:10.1023/a:1016099921195.

METEOALERTA Plan Nacional de Predicción y Vigilancia de Fenómenos Meteorológicos Adversos. METEOALERTA. Agencia Estatal de Meteorología (AEMET)http://www.aemet.es/documentos/es/eltiempo/prediccion/avisos/plan_meteoalerta/plan_meteoalerta.pdf2018(accessed 26 July 2019)

Morrison, H, Thompson, G, Tatarskii, V, 2009. Impact of cloud microphysics on the development of trailing stratiform precipitation in a simulated squall line: Comparison of one-and two-moment schemes. Mon. Weather Rev. 137 (3), 991–1007. doi:10.1175/2008mwr2556.1.

Moya-Alvarez, A S, Martínez-Castro, D, Flores, J L, Silva, Y, 2018. Sensitivity study on the influence of parameterization schemes in WRF_ARW model on short-and medium-range precipitation forecasts in the Central Andes of Peru. Adv. Meteorol.. doi:10.1155/2018/1381092.

Moya-Álvarez, A S, Gálvez, J, Holguín, A, Estevan, R, Kumar, S, Villalobos, E, Martínez-Castro, D, Silva, Y, 2018. Extreme rainfall forecast with the WRF-ARW model in the Central Andes of Peru. Atmosphere 9, 362. doi:10.3390/atmos9090362.

Moya-Álvarez, A S, Martínez-Castro, D, Kumar, S, 2019. Response of the WRF model to different resolutions in the rainfall forecast over the complex Peruvian orography. Theor Appl. Climatol 137, 2993–3007. doi:10.1007/s00704-019-02782-3.

Nakanishi, M, Niino, H, 2006. An improved Mellor–Yamada level-3 model: its numerical stability and application to a regional prediction of advection fog. Boundary-Layer Meteorol. 119 (2), 397–407. doi:10.1007/s10546-005-9030-8.

Pereira, C S, Carvalho, A C, Ferreira, J, Nunes, J P, Keizer, J J, Rocha, A, 2013. Simulation of a persistent medium-term precipitation event over the Western Iberian Peninsula. Hydrol. Earth Syst. Sci. Discuss. 10. doi:10.5194/hessd-10-1423-2013.

Pérez, C, Jiménez, P, Jorba, O, Sicard, M, Baldasano, J M, 2006. Influence of the PBL scheme on high-resolution photochemical simulations in an urban coastal area over the Western Mediterranean. Atmos. Environ. 40, 5274–5297. doi:10.1016/j.atmosenv.2006.04.039.

Pleim, J E, 2007. A combined local and nonlocal closure model for the atmospheric boundary layer. Part I: Model description and testing. J. Appl. Meteorol. Climatol. 46 (9), 1383–1395. doi:10.1175/jam2539.1.

Quitián-Hernández, L, Fernández-González, S, González-Alemán, J J, Valero, F, Martín, M L, 2018. Analysis of sensitivity to different parameterization schemes for a subtropical cyclone. Atmos. Res. 204, 21–36. doi:10.1016/j.atmosres.2018.01.001.

Sahoo, B, Bhaskaran, P K, Pradhan, A K, 2019. Application of weather forecasting model WRF for operational electric power network management—a case study for Phailin cyclone. Theor. Appl. Climatol. 137, 871–891. doi:10.1007/s00704-018-2639-6.

Skamarock, W C, Klemp, J B, Dudhia, J, Gill, D O, Barker, D, Duda, M G, Powers, J G, 2008. A Description of the Advanced Research WRF Version 3 (No. NCAR/TN-475+STR). University Corporation for Atmospheric Research. doi:10.5065/D68S4MVH.

Suárez-Molina, D, Fernández-Monistrol, J A, Uriel-González, A E, 2018. Catálogo-guía de fenómenos meteorológicos que afectan a la isla de Gran Canaria. Agencia Estatal de Meteorología. Ministerio para la Transición Ecológica, Madrid, p. 101 NIPO: 014-18-005-8.

Suárez-Molina, D, Fernández-González, S, Suárez González, J C, Oliver, A, 2020. Analysis of sounding derived parameters and application to severe weather events in the Canary Islands. Atmos. Res. 237, 104865. doi:10.1016/j.atmosres.2020.104865.

Tao, W K, Simpson, J, McCumber, M, 1989. An ice-water saturation adjustment. Mon. Weather Rev. 117 (1), 231–235. doi:10.1175/1520-0493(1989)117<0231:aiwsa>2.0.co;2.

Thompson, G, Field, P R, Rasmussen, R M, Hall, W D, 2008. Explicit forecasts of winter precipitation using an improved bulk microphysics scheme. Part II: Implementation of a new snow parameterization. Mon. Weather Rev. 136 (12), 5095–5115. doi:10.1175/2008mwr2387.

Winant, C D, Dorman, C E, Friehe, C A, Beardsley, R C, 1988. The marine layer off northern California: an example of supercritical channel flow. J. Atmos. Sci. 45, 3588–3605.

Žagar, Nedjeljka & Andersson, Erik & Fisher, Michael, 2005. Balanced tropical data assimilation based on study of equatorial waves in ECMWF short-range forecast errors.. Quarterly Journal of the Royal Meteorological Society 131, 987–1011. doi:10.1256/qj.04.54..

Zhao, B, Zhang, B, 2018. Assessing Hourly Precipitation Forecast Skill with the Fractions Skill score. J. Meteorol. Res. 32 (1), 135–145. doi:10.1007/s13351-018-7058-1.